



# Geodynamic regimes of intra-oceanic subduction: Implications for arc extension vs. shortening processes

Bettina Baitsch-Ghirardello <sup>a,\*</sup>, Taras V. Gerya <sup>a,b</sup>, Jean-Pierre Burg <sup>a</sup>

<sup>a</sup> Department of Earth Sciences, Swiss Federal Institute of Technology (ETH-Zurich), Sonneggstrasse, 5, 8092 Zurich, Switzerland

<sup>b</sup> Adjunct Professor of Geology Department, Moscow State University, 119899 Moscow, Russia

## ARTICLE INFO

### Article history:

Received 28 March 2012

Received in revised form 28 July 2012

Accepted 4 November 2012

Available online 23 November 2012

### Keywords:

Forearc subduction

Trench migration

Backarc extension

Rheological weakening effects

Numerical modeling

## ABSTRACT

40% of the subduction margins of the Earth are intra-oceanic. They show significant variability in terms of extension and shortening. We investigated numerically the physical controls of these processes using a 2D petrological-thermo-mechanical intra-oceanic subduction model with spontaneous volcanic arc growth and deformation. We varied the fluid- and melt-related weakening, the ages of both the subduction slab and the overriding plate, the subducting plate velocities, and the cohesive strength of rocks. Three main geodynamic regimes were identified: retreating subduction with opening of a backarc basin, stable subduction, and advancing, compressive subduction. The main difference between these regimes is the degree of rheological coupling between plates, which is governed by the intensity of rheological weakening induced by fluids and melts. Retreating subduction regimes require plate decoupling, which results from strong weakening due to both fluids and melts. Spreading centers nucleate either in forearc or in intraarc regions. Episodic trench migration is often due to variations of plate coupling with time, which is caused by (fore) arc deformation. Stable subduction regime with little variation in the trench position forms at an intermediate plate coupling and shows a transient behavior from the retreating to advancing modes. The advancing subduction regime results from strong plate coupling. At the mature stage, this subduction mode is associated with both partial fragmentation and subduction of the previously serpentinized forearc region. Forearc subduction is typically associated with a magmatic pulse, which is caused by dehydration of subducted serpentinized forearc fragments. Our models demonstrate distinct differences in thermal and lithological structure of subduction zones formed in these different geodynamic regimes. Results compare well with variations observed in natural intra-oceanic arcs.

© 2012 International Association for Gondwana Research. Published by Elsevier B.V. All rights reserved.

## 1. Introduction

Intra-oceanic subduction is a frequent plate tectonic process at the boundaries between converging oceanic plates. Intra-oceanic subduction zones (Fig. 1) comprise around 17,000 km, i.e. nearly 40%, of the subduction margins of the Earth (Leat and Larter, 2003). As a consequence, oceanic magmatic arcs are formed worldwide (Fig. 1) (Leat and Larter, 2003). Intra-oceanic subduction zones are sites of intense magmatic and seismic activity as well as metamorphic and tectonic processes shaping out arc compositions and structures. Despite their broad occurrence, intra-oceanic subduction zones and arcs are rather difficult to study since their major parts are principally below sea level, sometimes with only the tops of the largest volcanoes forming islands.

Intra-oceanic subduction zones show significant variability in terms of their structure and dynamics (Leat and Larter, 2003; Straub and Zellmer, 2012). Most of them currently function in *retreating*

mode (trench moves backward, rollback) (Stern, 2002, 2011) while the overriding plates are affected by various forearc, intra-arc and backarc extension/spreading processes. For example, the Mariana- and Izu–Bonin-arc systems include temporal series of magmatic arcs and basins (Stern, 2002, 2011). An important variable is the location of the spreading center. It may split the arc into two distinct parts (*intraarc extension*) and may create a thin oceanic lithosphere in between; this is the case for the Mariana Trough between the active Mariana arc and the inactive West Mariana Ridge. These observations are consistent with the seismic images of the Izu–Bonin–Mariana-arc (Takahashi et al., 2008, 2009) showing the new lithosphere with different thickness and crustal compositions along-strike of the arc-system (Kodaira et al., 2008, 2010). Examples of currently *advancing* subduction zones (trench migrates in the direction of the subduction) are the intra-oceanic arc-systems of the Aleutian, and Solomon (Leat and Larter, 2003). It is, therefore, important to understand how and where arc extension vs. compression initiate and evolve.

Arc extension and compression remain a debated subject from both natural observations (Leat and Larter, 2003) and modeling

\* Corresponding author.

E-mail address: [baitsch@erdw.ethz.ch](mailto:baitsch@erdw.ethz.ch) (B. Baitsch).

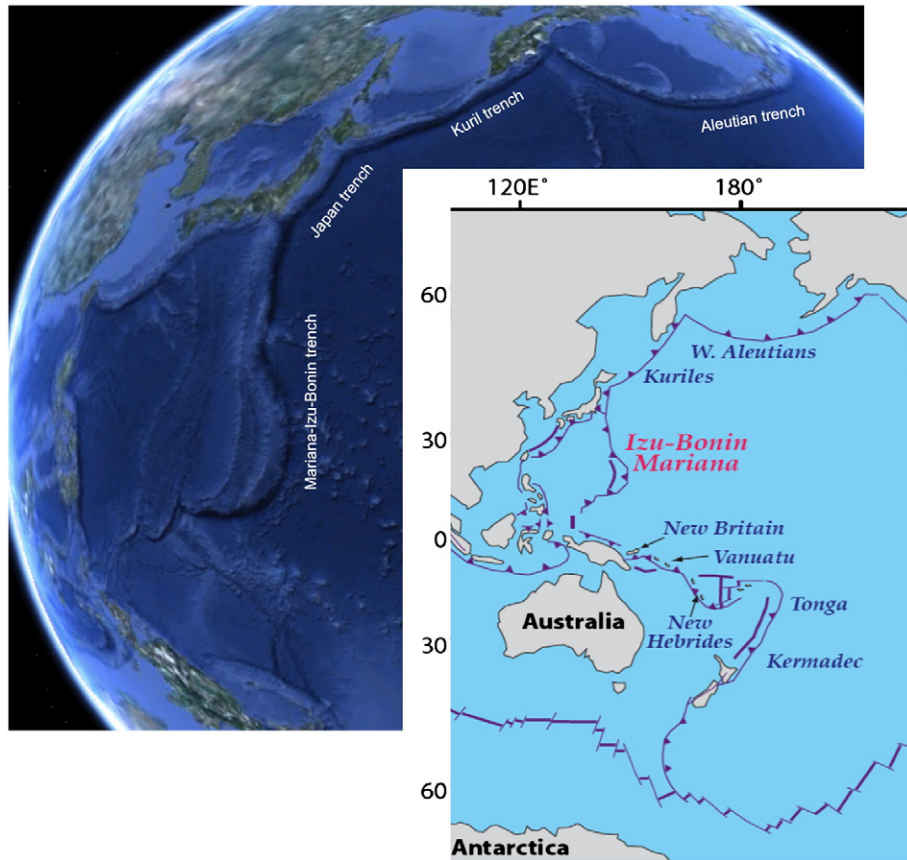


Fig. 1. Overview of major modern intra-oceanic subduction zones (based on Google Earth, Tatsumi and Stern, 2006).

(Arcay et al., 2005; Billen, 2008; Nikolaeva et al., 2008) points of view. Recent studies of intra-oceanic arcs focused on rheological variations (Arcay et al., 2005; Billen, 2008; Nikolaeva et al., 2008), plate motions (Sdrolias and Muller, 2006; Arcay et al., 2008; Clark et al., 2008), crustal growth (Kodaira et al., 2007; Takahashi et al., 2007, 2008; Lallemand et al., 2008; Nikolaeva et al., 2008; Zhu et al., 2009, 2011) and spatial and temporal evolutions (Miller et al., 2006). Several authors (Gerya et al., 2002; Arcay et al., 2005, 2008; Gorczyk et al., 2006) proposed that weakening and extension of the overriding plate are controlled by hydration/serpentinization reactions triggered by aqueous fluid released from the slab. Arcay et al. (2008) investigated the influences of subducting and overriding plate velocities on arc tectonic regimes and concluded that upper plate retreat (vs. advance) increases extension (vs. compression) in the arc lithosphere. Their modeling confirmed the statistical kinematic relationship that describes the transition from extensional to compressional stresses in the arc lithosphere (Lallemand et al., 2008). Arcay et al. (2008) also showed that the arc deformation mode is time-dependent on scales of millions to few tens of million years. Clark et al. (2008) investigated numerically the episodic behavior in trench motion and backarc tectonics based on simplified 3D models with freely subducting slabs. They defined three types of episodicity and found evidence of these in nature.

Shortening of intra-oceanic arcs received relatively little attention in terms of modeling. Boutelier et al. (2003) investigated with analog models different stages of arc and forearc subduction those that likely played important roles in collisional mountain belts such as the Himalayas and Tibet (Boutelier and Chemenda (2011) and references therein). These authors, in particular, argued that without the existence of a backarc (i.e. no thin and weak lithosphere in the rear of the arc), the overriding plate fails in the arc area. This may lead to forearc block subduction. So far, no numerical modeling has successfully complemented

these analog models. Only recently, Gerya and Meilick (2011) demonstrated numerically that in case of oceanic–continental (i.e. active margin) subduction geodynamic transition from arc compression to extension should be critically determined by the magnitude of rheological weakening induced by fluids and melts. These results are, however, not directly applicable to intra-oceanic subduction because of major differences in the overriding plate origin, composition and structure.

In this paper we aim to investigate numerically which physical parameters control the transition from compression to extension in intra-oceanic subduction. We performed systematic numerical experiments with a new 2D high-resolution petrological-thermo-mechanical subduction model including spontaneous intra-oceanic arc development and deformation. The results are analyzed with respect to fluid and melt weakening effects, cohesive strength of rocks, subducting plate velocity and plate ages. We classify three major intra-oceanic subduction regimes and present their implications for arc extension and compression, forearc subduction and trench migration.

## 2. Numerical model description

Our modeling approach is comparable to that of (Sizova et al., 2010) and Gerya and Meilick (2011) who presented numerical details not provided here. The model is based on the 2D thermo-mechanical I2ELVIS code (Gerya and Yuen, 2003a, 2003b, 2007) based on finite differences and marker-in-cell method.

### 2.1. Model design

The 2D numerical model (Fig. 2) simulates subduction of an oceanic plate beneath another oceanic plate. The model starts with subduction initiation and spans a period equivalent to about 40 Ma.

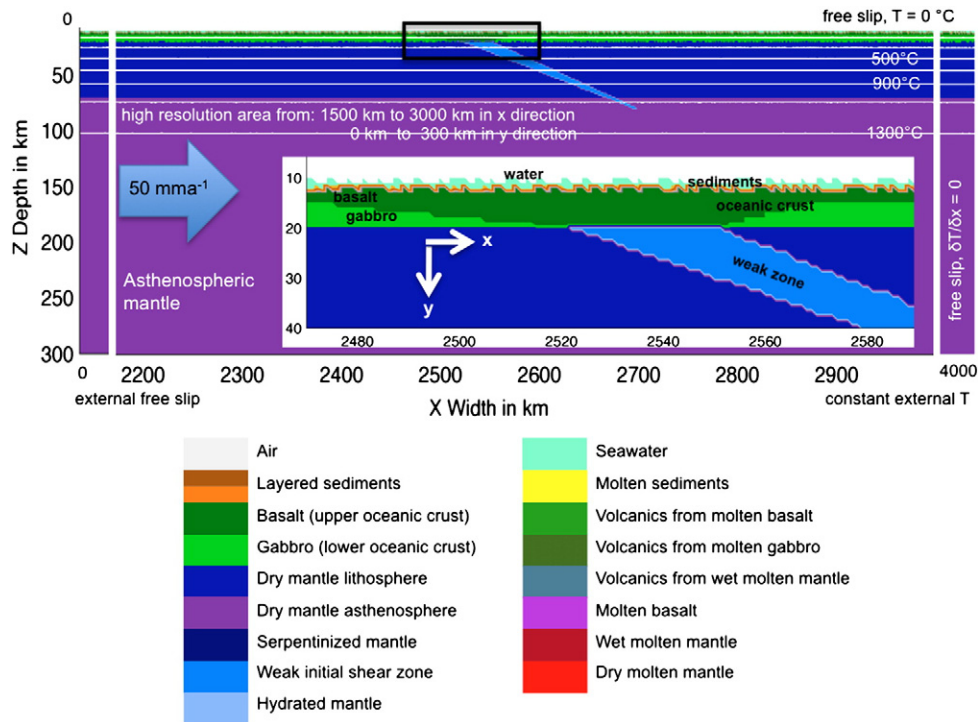


**Fig. 2.** Initial numerical model setup. Staggered grid resolution =  $2001 \times 301$  nodal points, with more than 10 million randomly distributed markers. Grid step is  $1 \times 1$  km in the subduction zone area (1500–3000 km) and  $5 \times 5$  km outside of this area. Prescribed subducting plate velocity remains constant during the entire experiment. Isotherms (white lines) from  $100$  °C with  $200$  °C intervals. Material colors for all figures. Two layers in the sediments and the mantle have same physical properties but are differently colored to better visualize deformation.

The scaled size of the model is 300 km in depth and 4000 km in length with the subducting plate being about 2500 km long and the overriding plate 1500 km (Fig. 2). The rectangular non-uniform  $2001 \times 301$ -node-grid contains a 1500 km long (from  $x = 1500$  km to  $x = 3000$  km, Fig. 2), high resolution ( $1 \times 1$  km) mesh refinement area in the middle of the model. The resolution is  $5 \times 1$  km over the

rest of the model. The oceanic crusts of both the subducting and overriding plates represent an upper layer of hydrothermally altered basalts (2 km thick) overlying a 5 km thick layer of gabbro. The mantle consists of anhydrous peridotite (material properties in Table 1). The initiation of subduction is prescribed by an initially weak zone with wet olivine rheology and low brittle/plastic strength ( $\sin\phi = 0.1$  where  $\phi$  is the effective

**Table 1**  
Physical properties of rocks<sup>a</sup> used in numerical experiments.

Material	$\rho_0$ , $\text{kg m}^{-3}$	$k$ , $\text{W m}^{-1} \text{K}^{-1}$ (at $T_K$ , $P_{\text{MPa}}$ )	$T_{\text{solidus}}$ , K (at $P_{\text{MPa}}$ )	$T_{\text{liquidus}}$ K (at $P_{\text{MPa}}$ ),	Latent heat ( $\text{kJ kg}^{-1}$ )	Radioactive heating ( $\mu\text{Wm}^{-3}$ )	Flow law
Sediments, volcanics from sediments	2600(solid) 2400(molten)	$[0.64 + 807/(T+77)] \cdot \exp(0.00004P)$	$889 + 17,900/(P+54) + 20,200/(P+54)^2$ at $P < 1200$ MPa, $831 + 0.06P$ at $P > 1200$ MPa	$1262 + 0.09P$	300	2	Wet quartzite, $c = 10$ MPa, $\sin(\phi_{\text{dry}}) = 0.15$
Upper oceanic crust (basalt)	3000(solid) 2900(molten)	$[1.18 + 474/(T+77)] \cdot \exp(0.00004P)$	$973 + 70,400/(P+354) + 778,00,000/(P+354)^2$ at $P < 1600$ MPa, $935 + 0.0035P + 0.0000062P^2$ at $P > 1600$ MPa	$1423 + 0.105P$	380	0.25	Wet quartzite, $c = 10$ MPa, $\sin(\phi_{\text{dry}}) = 0.1$
Lower oceanic crust (gabbro)	3000(solid) 2900(molten)	$[1.18 + 474/(T+77)] \cdot \exp(0.00004P)$	$973 + 70,400/(P+354) + 778,00,000/(P+354)^2$ at $P < 1600$ MPa, $935 + 0.0035P + 0.0000062P^2$ at $P > 1600$ MPa	$1423 + 0.105P$	380	0.25	Plagioclase $\text{An}_{75}$ , $c = 10$ MPa, $\sin(\phi_{\text{dry}}) = 0.6$
Volcanics from wet molten mantle and subducted basalts and gabbro	3000(solid) 2900(molten)	$[1.18 + 474/(T+77)] \cdot \exp(0.00004P)$	$973 + 70,400/(P+354) + 778,00,000/(P+354)^2$ at $P < 1600$ MPa, $935 + 0.0035P + 0.0000062P^2$ at $P > 1600$ MPa	$1423 + 0.105P$	380	0.25	Wet quartzite, $c = 10$ MPa, $\sin(\phi_{\text{dry}}) = 0.15$
Lithosphere– asthenosphere dry mantle	3300(solid) 2900(molten)	$[0.73 + 1293/(T+77)] \cdot \exp(1 + 0.00004P)$	$1394 + 0.132899P - 0.000005104P^2$ at $P < 10,000$ MPa, $2212 + 0.030819(P - 10,000)$ at $P > 10,000$ MPa	$2073 + 0.114P$	400	0.022	Dry olivine, $c = 10$ MPa, $\sin(\phi_{\text{dry}}) = 0.6$
Lithosphere– asthenosphere wet mantle	3000(serpentinized) 3200(hydrated <sup>b</sup> ) 2900(molten)	$[0.73 + 1293/(T+77)] \cdot \exp(1 + 0.00004P)$	$1240 + 49,800/(P+323)$ at $P < 2400$ MPa, $1266 - 0.0118P + 0.0000035P^2$ at $P > 2400$ MPa	$2073 + 0.114P$	400	0.022	Wet olivine, $c = 10$ MPa, $\sin(\phi_{\text{dry}}) = 0.1$
References <sup>c</sup>	1,2	3,9	4,8	4	1,2	1	10

<sup>a</sup> Other properties (for all rock types):  $C_p = 1000 \text{ J kg}^{-1} \text{K}^{-1}$ ,  $\alpha = 3 \cdot 10^{-5} \text{ K}^{-1}$ ,  $\beta = 1 \cdot 10^{-5} \text{ MPa}^{-1}$ .

<sup>b</sup> Hydrated mantle beyond the antigorite stability field (Schmidt & Poli, 1998):  $T_K > 751 + 0.18P - 0.000031P^2$  at  $P < 2100$  MPa,  $T_K > 1013 - 0.0018P - 0.0000039P^2$  at  $P > 2100$  MPa.

<sup>c</sup> 1 = Turcotte & Schubert (2002); 2 = Bittner & Schmeling (1995); 3 = Clauser & Huenges (1995); 4 = Schmidt & Poli (1998); 5 = Hess (1989); 6 = Hirschmann (2000); 7 = Johannes (1985); 8 = Poli & Schmidt (2002); 9 = Hofmeister (1999); 10 = Ranalli (1995).

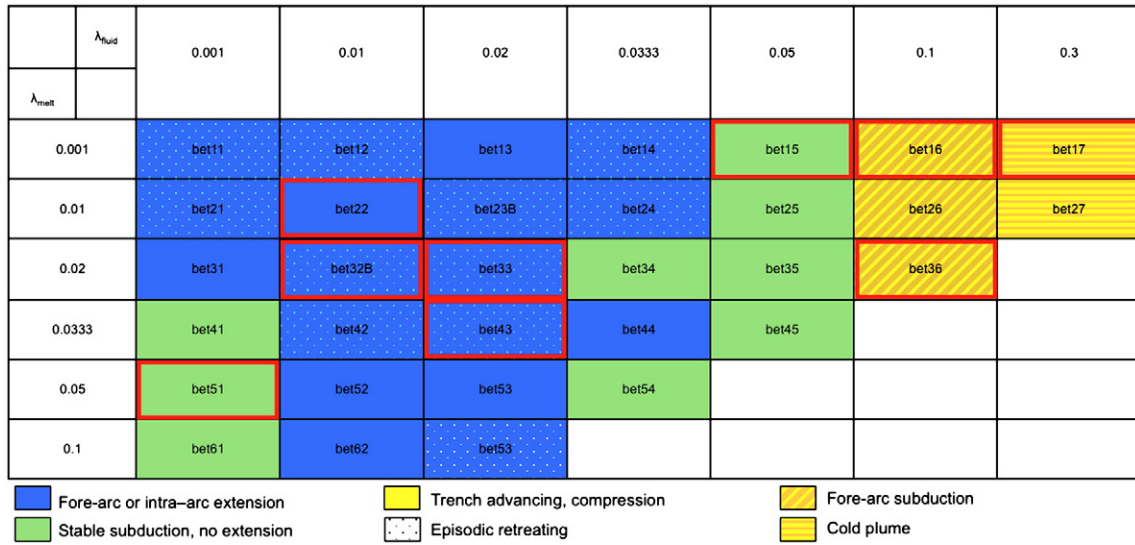


**Fig. 3.** Area diagram reporting the investigated models in terms of arc extension (blue), stable subduction (green) and arc compression (yellow) with forearc subduction (diagonal hatching) and/or cold plume (horizontal hatching) in function of fluid- ( $\lambda_{fluid}$ ) and melt- ( $\lambda_{melt}$ ) weakening effects. White dots stand for episodic trench retreat. Reference models discussed in the text are framed in red.

internal friction angle) (Fig. 2). An internally prescribed velocity field within the convergence condition region drives the spontaneously bending slab during the entire duration of the experiment.

The mechanical boundary conditions are free slip at the top and side boundaries, whereas the lower boundary is permeable in the vertical direction (Gorczyk et al., 2007a, 2007b). The top surface of the lithosphere is treated as an internal free erosion/sedimentation

surface (e.g. Gorczyk et al., 2007b; Schmeling et al., 2008) by using an 8–12.5 km thick top layer with low viscosity ( $10^{18}$  Pa s) and density ( $1 \text{ kg/m}^3$  for air above  $y = 10 \text{ km}$  level,  $1000 \text{ kg/m}^3$  for sea water below  $y = 10 \text{ km}$  level). Large scale erosion ( $0.3 \text{ mm/a}$ ) and sedimentation ( $0.03 \text{ mm/a}$ ) rates were used to account for the effects of erosion and sedimentation on the topographical evolution above and below the sea water level, respectively (Gorczyk et al., 2007a, 2007b).

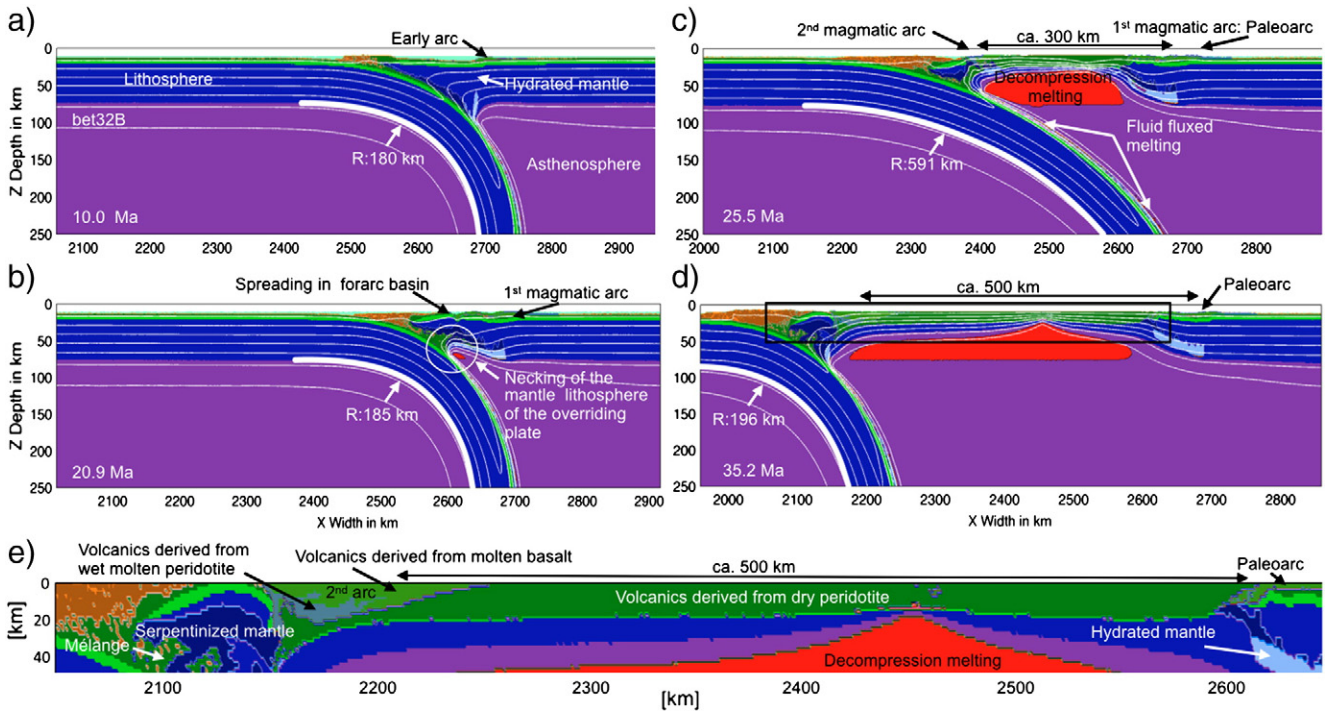


**Fig. 4.** Reference model for the retreating subduction regime; ( $\lambda_{fluid} = 0.01$  and  $\lambda_{melt} = 0.02$ , model bet32B in Fig. 2). Time 0 = beginning of convergence. Calculation mode of curvature from Vogt et al. (2012). Radius of curvature R measured at a lithospheric depth of 70 km (thick white line). (a): Early arc established above the hydrated mantle region; (b): Establishment of a spreading center in the forearc; (c) and (d): Decompression melting producing a new MORB crust in back-arc regions and separating a paleo arc from the next-to-trench active arc. (e): Zoom of (d) showing the new arc derived from molten wet peridotite and molten basalt.

## 2.2. Hydration process

Like in previous petrological–thermomechanical subduction models, we used thermodynamic database to account for slab dehydration and mantle wedge hydration (e.g., Riepke et al., 2004; Hebert et al., 2009; Gerya and Meilick, 2011). In addition to mineralogical water computed from the database (Gerya and Meilick, 2011), H<sub>2</sub>O is also present as a free porous fluid making up to 2 wt.% in sediments and hydrothermally altered basalt. The pore water content is supposed to decrease linearly from the maximal value of 2 wt.% at the surface to 0 wt.% at 75 km depth. The release of this water also mimics effects of low-temperature (T < 573 K) reactions, which are not included in our thermodynamic database.

The slab is being dehydrated as it sinks. The timing of H<sub>2</sub>O release by dehydration reactions is determined by the physicochemical conditions of the model and the assumption of thermodynamic equilibrium. Water propagation is modeled in the form of water markers moving upward with an assumed water percolation velocity of 10 cm/a, which is similar to previous subduction models and allows for efficient water transport from the slab to the mantle wedge (Gorczyk et al., 2007b; Hebert et al., 2009; Sizova et al., 2010; Gerya and Meilick, 2011). The marker releases water as soon as it encounters a rock capable of absorbing water by hydration or melting reactions at given PT-conditions and rock composition (Gorczyk et al., 2007b; Nikolaeva et al., 2008; Sizova et al., 2010).

## 2.3. Partial melting and melt extraction processes

Because the H<sub>2</sub>O transport model does not permit complete hydration of the peridotite mantle, the mantle solidus is intermediate between the wet and dry peridotite solidi. To account for this behavior, we assume that the degree of both hydrous and dry melting is a linear function of pressure and temperature (e.g. Gerya and Yuen, 2003a). In this model the standard (i.e. without melt extraction) volumetric degree of melting  $M_0$  is,

$$M_0 = 0 \quad \text{when } T < T_{\text{solidus}};$$

$$M_0 = (T - T_{\text{solidus}}) / (T_{\text{liquidus}} - T_{\text{solidus}}) \quad \text{when } T_{\text{solidus}} < T < T_{\text{liquidus}};$$

$$M_0 = 0 \quad \text{when } T > T_{\text{liquidus}};$$

where  $T_{\text{solidus}}$  is the solidus temperature (wet and dry solidi are used for the hydrated and dry mantle, respectively) and  $T_{\text{liquidus}}$  is the dry liquidus temperature at a given pressure and rock composition (Table 1). To simulate melt extraction from partially molten rocks (e.g. Nikolaeva et al., 2008; Sizova et al., 2010) we define a melt extraction threshold  $M_{\text{max}} = 4\%$  and a non-extractable amount of melt  $M_{\text{min}} = 2\%$  that remains in the source. Extracted melts are assumed to propagate instantaneously and vertically toward the surface and build up a new volcanic crust (Nikolaeva et al., 2008; Sizova et al., 2010; Gerya and Meilick, 2011).

## 2.4. Rheological model

The effective stress- and temperature-dependent creep viscosity of rocks is computed according to experimentally determined flow laws (Ranalli, 1995) (Table 1). In our model, both fluid and melt propagation affect the brittle/plastic strength of rocks. This is implemented by including fluid and melt influences into the Mohr–Coulomb yield criterion as follows

$$\sigma_{\text{yield}} = c + P_{\text{solid}} \sin(\varphi),$$

$$\sin(\varphi) = \sin(\varphi_{\text{dry}}) \lambda_{\text{fluid}} \quad \text{and} \quad \lambda_{\text{fluid}} = 1 - P_{\text{fluid}}/P_{\text{solid}} \quad \text{in the regions of fluid percolation,}$$

$$\sin(\varphi) = \sin(\varphi_{\text{dry}}) \lambda_{\text{melt}} \quad \text{and} \quad \lambda_{\text{melt}} = 1 - P_{\text{melt}}/P_{\text{solid}} \quad \text{in the regions of melt percolation.}$$

Thus, the local brittle/plastic strength of a rock  $\sigma_{\text{yield}}$  depends on (1) the mean stress (pressure)  $P_{\text{solid}}$  on the solid, (2) the cohesion,  $c$ , which is the strength at  $P_{\text{solid}} = 0$ , and (3) the effective internal friction angle,  $\varphi$ , which is calculated from the friction angle of dry rocks,  $\varphi_{\text{dry}}$  (for values of  $c$  and  $\sin(\varphi_{\text{dry}})$  see Table 1), and the pore fluid/melt pressure factors  $\lambda_{\text{fluid}}/\lambda_{\text{melt}}$ . According to our model, the pore fluid pressure  $P_{\text{fluid}}$  reduces the yield strength of rocks subjected to percolation of water markers released from the slab. Similarly, ascending extracted melts reduce the yield strength in the column of rock between the source of the melt and the surface.  $\lambda_{\text{fluid}}$  and  $\lambda_{\text{melt}}$  factors are systematically varied in different numerical experiments.

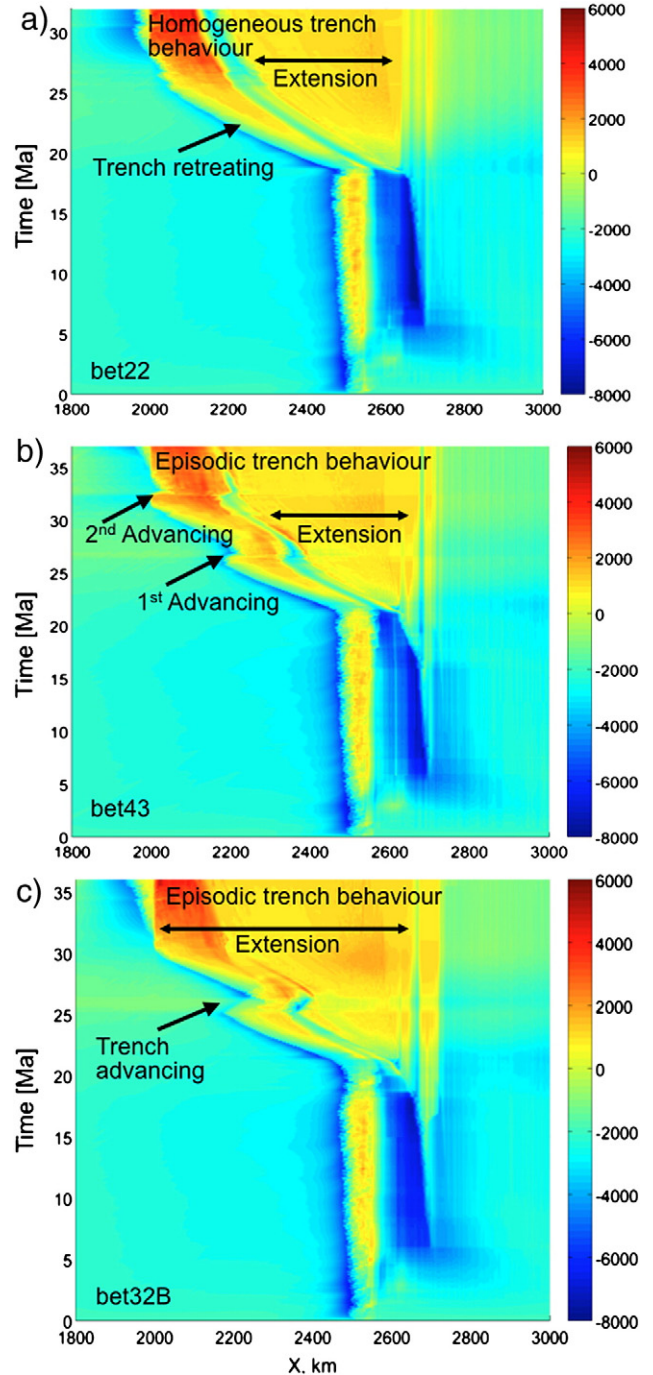
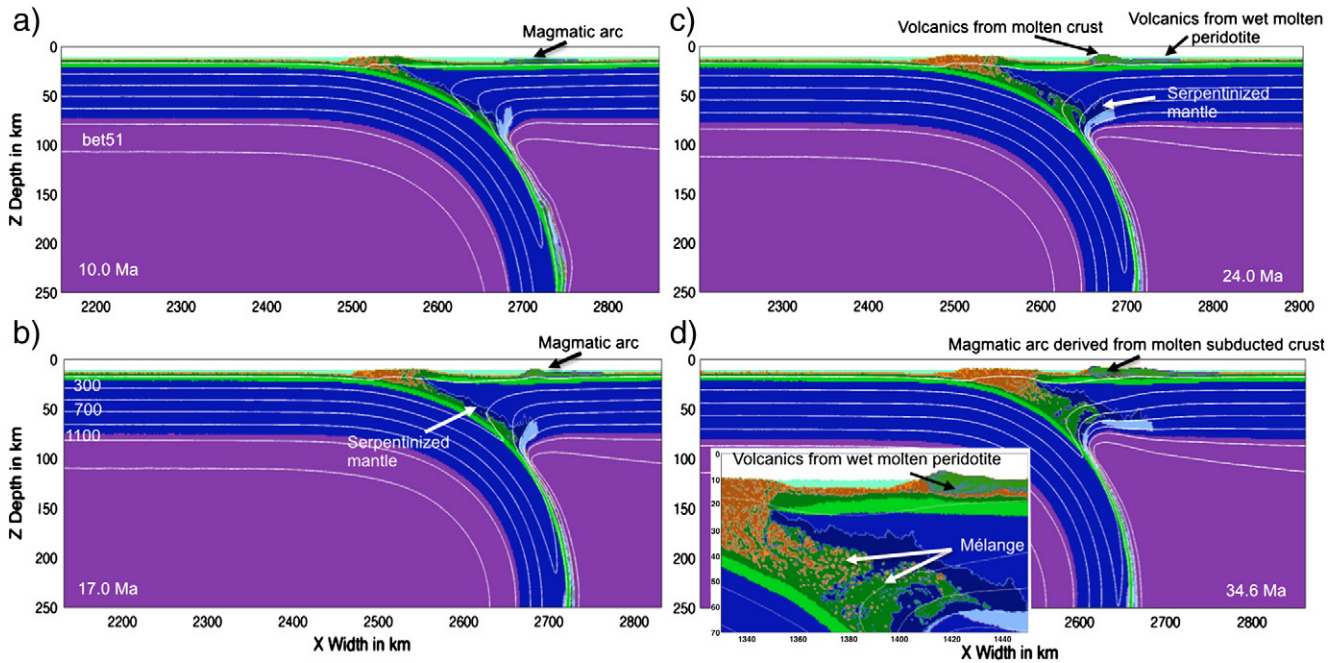


Fig. 5. Topography history for three retreating subduction models (Fig. 2). (a): Homogeneous trench retreat of about 510 km in 11 Ma (model bet22); (b): Episodic trench retreat (model bet43) with two short episodes of trench advance; (c): Episodic trench retreat with one short advance episode (model bet32B).



**Fig. 6.** Reference model for stable subduction and broad mélangé zone; ( $\lambda_{\text{fluid}} = 0.001$  and  $\lambda_{\text{melt}} = 0.05$ , model bet51 in Fig. 2). (a): Magmatic arc established 5 to 10 Ma after subduction initiation above of the hydrated mantle region; (b) and (c): Serpentinized area atop of the slab growing with time; (d): Broad area of mélangé of mechanically mixed subducted basaltic crust and serpentinized forearc mantle. Well developed magmatic arc, mainly derived from the molten subducted oceanic crust and molten hydrated mantle.

### 3. Results

#### 3.1. Geodynamic regimes of subduction

We performed 42 experiments by varying the following model parameters: fluid and melt related weakening ( $\lambda_{\text{fluid}}$ : 0.001, 0.01, 0.02, 0.0333, 0.05, 0.1, 0.3 and  $\lambda_{\text{melt}}$ : 0.001, 0.01, 0.02, 0.0333, 0.05, 0.1, 1.0), age of subducting (40, 140 Ma) and overriding (20, 40 Ma) lithosphere as well as prescribed constant subducting plate velocity ( $35 \text{ mm a}^{-1}$ ,  $50 \text{ mm a}^{-1}$  or  $85 \text{ mm a}^{-1}$ ) and brittle/plastic strength

of the mantle ( $\sin(\varphi_{\text{dry}})$ : 0.5, 0.6, 0.7). In agreement with previous models (Sizova et al., 2010), our results show that fluid and melt weakening are the most important parameters controlling the subduction regime. We distinguish three regimes depending on the conditions and experimental results (Fig. 3): (1) the retreating regime with either stable or episodic overriding plate extension (in the latter case alternation of trench retreat, trench advance, and quiescence episodes is observed), (2) the stable regime without compression and extension and (3) the advancing regime with forearc subduction. Reference models for these three regimes are now described.

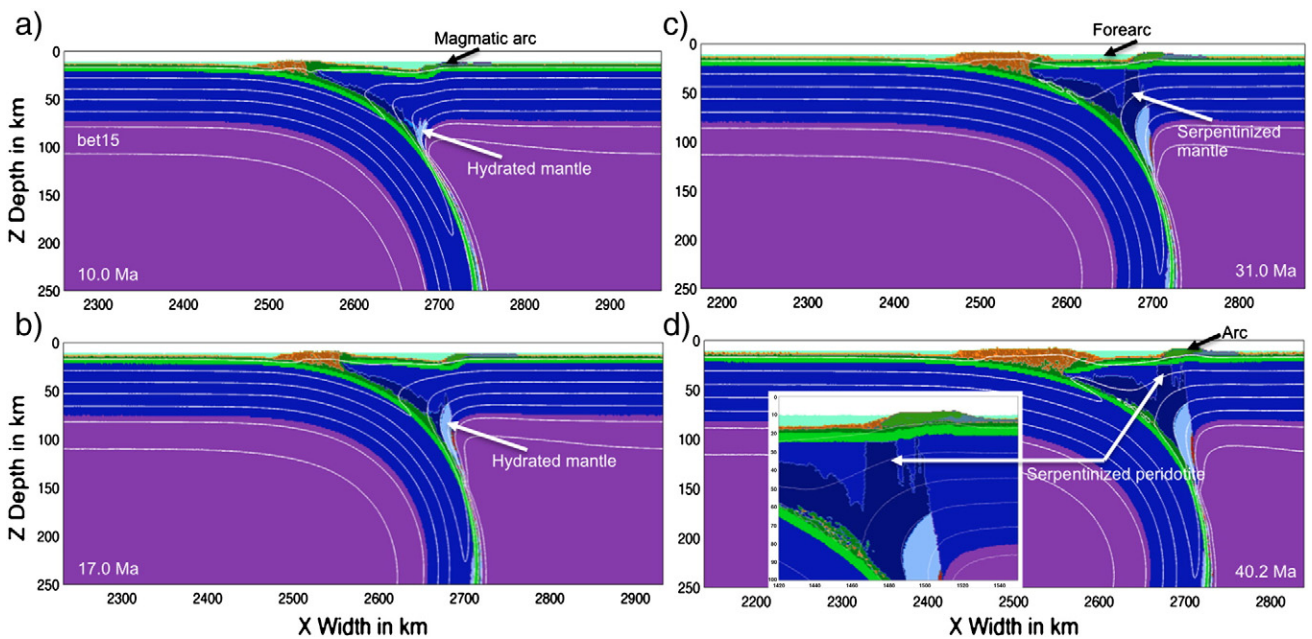


**Fig. 7.** Reference model for stable subduction; ( $\lambda_{\text{fluid}} = 0.05$  and  $\lambda_{\text{melt}} = 0.01$ , model bet15 in Fig. 2). (a): Narrow serpentinite mélangé area and magmatic arc above of a small area of hydrated mantle; (b)–(d): Broad serpentinization area in the forearc mantle due to the dehydration of the slab.

### 3.1.1. Retreating subduction regime

The retreating subduction regime occurs in experiments with strong weakening of the overriding plate by both fluids and melts ( $\lambda_{\text{fluid}}=0.001\text{--}0.0333$ ,  $\lambda_{\text{melt}}=0.001\text{--}0.05$ ) (Fig. 3). Model bet32B with  $\lambda_{\text{fluid}}=0.01$ ,  $\lambda_{\text{melt}}=0.02$  (Fig. 4) is our reference model of this subduction regime. In this model, the magmatic arc begins to grow 5 to 6 Ma after initiation of subduction. The arc volcanic rocks stem from the molten hydrated peridotite of the mantle wedge and from a small amount of molten basalt and gabbro of the subducted plate (Fig. 4a). The slab plunges with a strong curvature ( $R=185$  km; in all models the radii of curvature are measured at a depth of 70 km within the dry mantle). Extension in the fore/intra-arc region starts at about 20 Ma (Fig. 4b) after rheological weakening of the overriding plate mantle by hydration/serpentinization and melt propagation. Lowered viscosity of serpentinized forearc mantle (dark blue in Fig. 4b) together with melt-induced weakening of the arc lithosphere ( $\lambda_{\text{melt}}=0.02$ ) triggers localized extensional deformation (necking) of the overriding plate above the upper-left corner of the asthenospheric mantle wedge (white circle in Fig. 4b). Necking of the (fore) arc lithosphere (Fig. 4b) triggers decompression melting in the mantle wedge, and a basin opens at 30–50 km behind the accretionary wedge, 50–80 km in front of the first arc. Decompression melting generates a new oceanic lithosphere with a crust composition analog to MORB (Fig. 4c). As a consequence of decoupling and extension of the overriding plate, the trench starts to retreat. The initially strong curvature of the slab notably decreases from  $R=185$  km to  $R=591$  km during  $\sim 5$  Ma of trench retreat. This slab behavior is due to the transient rapid motion of the retreating arc (Fig. 4b,c). During trench retreat, a broad decompression melting region forms beneath the widening backarc basin (Fig. 4c,d). The frontal arc remains active and migrates together with the trench (Figs. 4a, 5c) at ca. 25 Ma, (Fig. 4c). The rear side becomes an extinct paleo-magmatic arc composed of subduction-related volcanics behind the back arc basin. The retreating trench position and the width of the back arc basin stabilize at about 35 Ma, which also results in steepening of the slab (the curvature increases toward the steady state  $R=196$  km; Fig. 5d).

Trench retreat is often irregular and one or several episodes of trench advance intervene (Fig. 5). These episodes are mainly caused by temporal variations in the degree of rheological coupling between the plates. Rheological coupling changes with time due to the ongoing deformations in the continuously serpentinized, heterogeneous forearc and subduction channel (Fig. 4d).

### 3.1.2. Stable subduction regime

Stable subduction regimes develop in two distinct areas of the investigated  $\lambda_{\text{fluid}}\text{--}\lambda_{\text{melt}}$  parameter space (Fig. 3): (i) stable subduction with wide serpentinite mélanges (Fig. 6) develops in experiments with strong fluid weakening combined with moderate melt weakening ( $\lambda_{\text{fluid}}\leq 0.001$ ,  $\lambda_{\text{melt}}\geq 0.0333$ ) and (ii) stable subduction with narrow serpentinite mélanges (Fig. 7) develops in experiments with moderate fluid weakening. The corresponding reference models are bet51 ( $\lambda_{\text{fluid}}=0.001$ ,  $\lambda_{\text{melt}}=0.05$ , Fig. 6) and bet15 ( $\lambda_{\text{fluid}}=0.05$ ,  $\lambda_{\text{melt}}=0.001$ , Fig. 7). A magmatic arc takes place approximately 5 to 10 Ma after subduction initiation. Like for the retreating subduction regime, the volcanic rocks are mainly produced from the molten hydrated mantle and the subducted oceanic crust (Figs. 4 and 6). Model bet51 is characterized by the development of a broad mélange area in which the subducted basaltic crust is mechanically mixed with the serpentinized forearc mantle (Fig. 6d). Intense mixing is promoted by an increased degree of fluid-related weakening that reduces the effective viscosity of the mélange (Gerya and Stockhert, 2002). In contrast, the mélange area in model bet15 is confined to the slab interface while the remaining parts of serpentinized forearc remain relatively undeformed. Their increased effective viscosity reflects a reduced degree of fluid weakening (Fig. 7d). The increased viscosity also increases coupling between the plates and results in a noticeable subsidence of the forearc. This is reflected in a deeper forearc basin in model bet15 than in model bet51 (cf. Fig. 8a and b). Although there is massive serpentinization and hydration of the forearc, there is no necking and extension of the overriding plate (Figs. 6b, 7b). Moreover, the subducting slab remains relatively steep ( $R=137\text{--}194$  km in bet15 and  $150\text{--}176$  km in bet51) and if there is trench retreat, it is for no more than 50 km over 35 Ma (Fig. 8a). The minor trench retreat is mainly caused by sediment accretion in the growing accretionary wedge (Figs. 6 and 7).

### 3.1.3. Advancing subduction regime

The advancing subduction regime develops under conditions of notably reduced fluid-related weakening ( $\lambda_{\text{fluid}}\geq 0.1$ , Fig. 3), which trigger strong coupling between the plates. At  $\lambda_{\text{fluid}}=0.1$  advancing subduction always induces forearc subduction (Figs. 9 and 10). At  $\lambda_{\text{fluid}}=0.3$ , forearc subduction becomes incomplete (Fig. 11). bet16 ( $\lambda_{\text{fluid}}=0.1$ ,  $\lambda_{\text{melt}}=0.001$ , Fig. 9) and bet36 ( $\lambda_{\text{fluid}}=0.1$ ,  $\lambda_{\text{melt}}=0.02$ , Fig. 10) are the reference models of advancing subduction. bet16 shows forearc subduction combined with folding of the overriding crust (both basalt

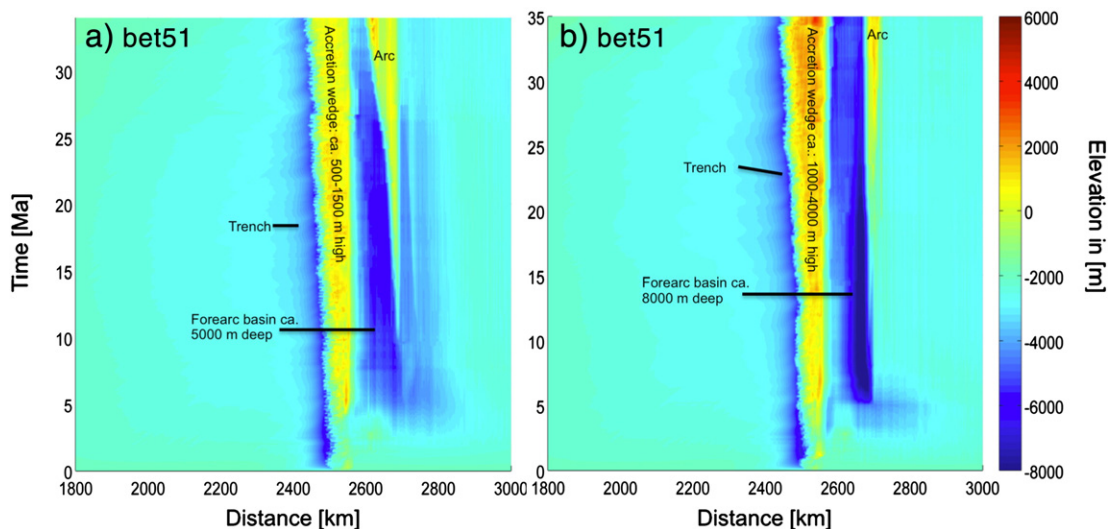
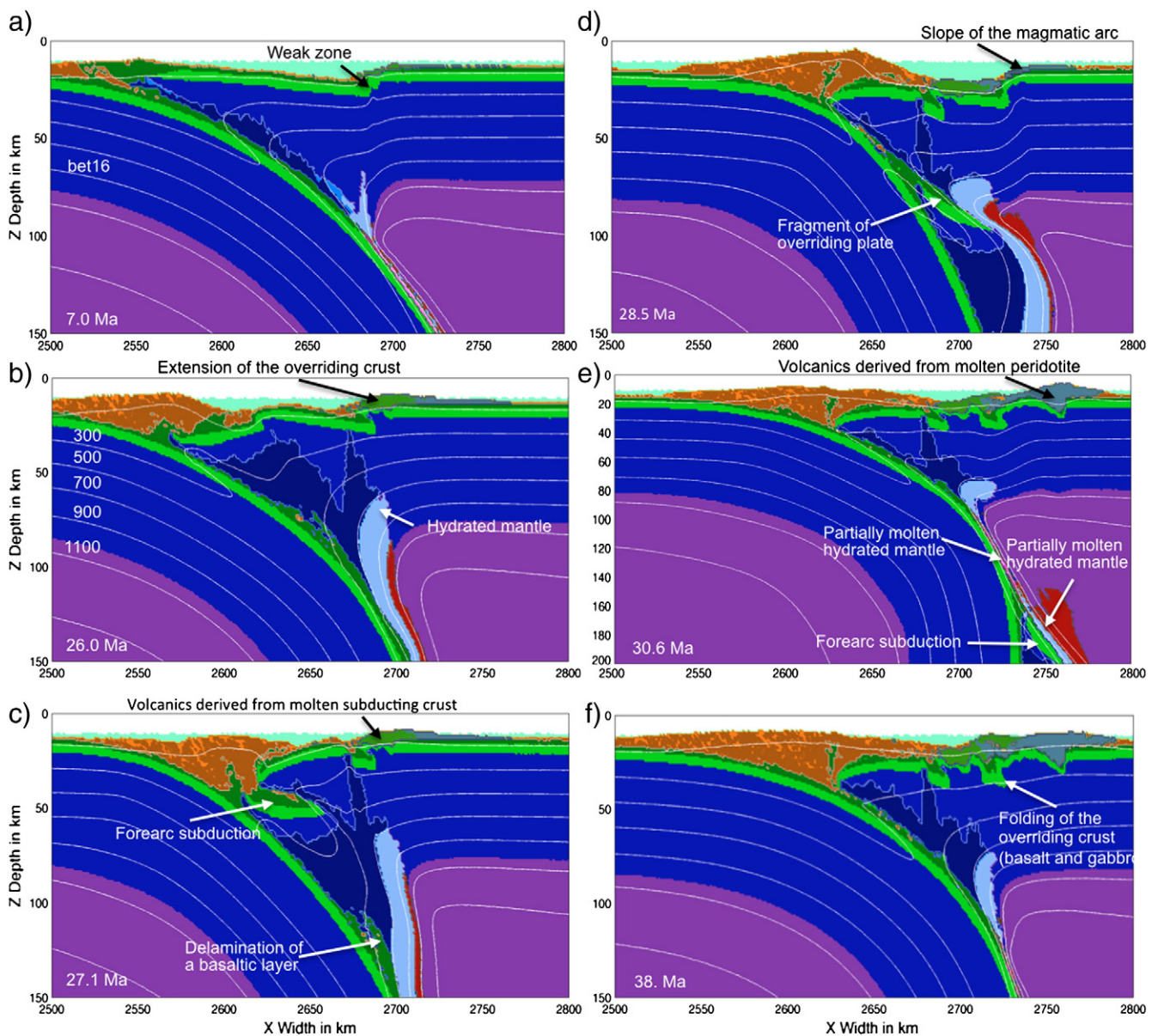


Fig. 8. Topography history of two stable subduction models (Fig. 2). (a): bet51 ( $\lambda_{\text{fluid}}=0.001$  and  $\lambda_{\text{melt}}=0.05$ ); (b): bet15 ( $\lambda_{\text{fluid}}=0.05$  and  $\lambda_{\text{melt}}=0.001$ ). Note differences in depth of the forearc basin and amount of incoming sediments in the accretionary wedge. Colorbar: Elevation in m.

and gabbro layers), whereas model bet36 shows forearc subduction without folding. Like in the retreating and stable regimes, the magmatic arc begins to grow 5 to 6 Ma after subduction initiation (Figs. 5, 8, 12). As in stable subduction models, the forearc basin develops during the first 25 Ma, after which forearc subduction starts (Figs. 9c, 12a,b). Forearc subduction produces a strong change in topography dynamics (Fig. 12a). It also involves gradual mechanical disintegration of the forearc mantle by heterogeneous serpentinization (Fig. 9a–c). Strong coupling between plates builds up large stresses able to overcome the mechanical resistance of the serpentinized forearc mantle, which becomes subducted together with the subduction plate at around 27 Ma (Fig. 9d). The upper bound of the subducted forearc crust lies typically under the slope of the magmatic arc (Figs. 9d,e, 10c,d), which leads to the almost complete closure of the forearc basin (Figs. 10c, 12a,b). The detailed dynamics of forearc subduction (Fig. 9c,d) demonstrates complex interactions between different parts of the overriding plate. Deep forearc subduction (~150 km depth, Fig. 9e) results in transient

enhanced magmatic activity caused by water release from the subducted forearc serpentinized mantle at asthenospheric depths at around 31 Ma. Large amounts of new basaltic crust form at the surface as the result of enhanced fluid-fluxed melting of the mantle wedge (Fig. 9f). Such deep forearc subduction only develops in models with  $\lambda_{fluid} = 0.1$  (~25 Ma). At  $\lambda_{fluid} = 0.3$ , forearc subduction becomes incomplete (Fig. 11, bet17) and is replaced by shallow (in 15–30 km depth) buckling/shortening (~15 Ma) of the serpentinized forearc mantle (Fig. 11). In experiment bet17 ( $\lambda_{fluid}$ : 0.3 and  $\lambda_{melt}$ : 0.001), advancing subduction accompanies forearc shortening and the development of a deep (100–120 km) thermal–chemical plume composed of partially molten subducted sediments and basalts as well as partially molten hydrated mantle. In agreement with previous subduction models (e.g. Gerya and Meilick, 2011), the development of sedimentary plumes is associated with strong plate coupling and increased subduction erosion of sediments. The characteristic thickening of the subducted



**Fig. 9.** Reference model for forearc subduction; ( $\lambda_{fluid} = 0.1$  and  $\lambda_{melt} = 0.001$ , model bet16 in Fig. 2). Zoomed area: (a) Weak zone below the magmatic arc. (b): Initiation of plate breaking. Hydration and serpentinization of the forearc mantle; (c): Second breaking and subduction of the first fragment; (e): Subduction of the broken forearc with the subducting slab; (f): Broad area of flux melting feeding the magmatic arc. Buckling of the thin overriding crust. (g) Magmatic arc mainly derived from partially molten peridotite, decreases. The forearc basin contracts.

sediments triggers the development of buoyant, partially molten trans-lithospheric cold plumes atop the slab. The rock composition of the arc in model bet17 is heterogeneous since it has been extracted from molten gabbro, basalt, sediments, and peridotite.

### 3.2. Influence of model parameters

#### 3.2.1. Influence of plate ages

We varied cooling ages of both subducting (40–140 Ma) and overriding (20–40 Ma) plates in the retreating subduction models bet11, bet21, and bet22 (Fig. 3). Results suggest that the slab age has rather small effects on spreading initiation, which takes longer (20–21 Ma) in models with contrasting plate ages (Fig. 13b,c) than in the reference model (17 Ma, Fig. 13a). On the other hand, spreading rates positively correlate with the slab age (and thus with the magnitude of

negative slab buoyancy compared to the asthenosphere) and are up to 3 times higher in models with 140 Ma old slabs ( $164 \text{ mm a}^{-1}$  spreading rate, Fig. 13b right column) than with 40 Ma old slabs ( $48\text{--}66 \text{ mm a}^{-1}$  spreading rate, Fig. 13a,c right column).

#### 3.2.2. Influence of subducting plate velocity

We varied the prescribed constant subducting plate velocity, which is maintained during the entire experiment, from 35 to 85 mm/a for models bet11, bet21 and bet22 (Fig. 3) under conditions of contrasting cooling ages of subducting (140 Ma) and overriding (40 Ma) plates. An increase of the subducting plate velocity leads to earlier initiation of a spreading center (Fig. 14a/b/c). Indeed, the amount of plate convergence needed for spreading initiation increases with decreasing subducting plate velocity from 800 to 900 km in the models with 85 mm/a velocity to 1200–1400 km in

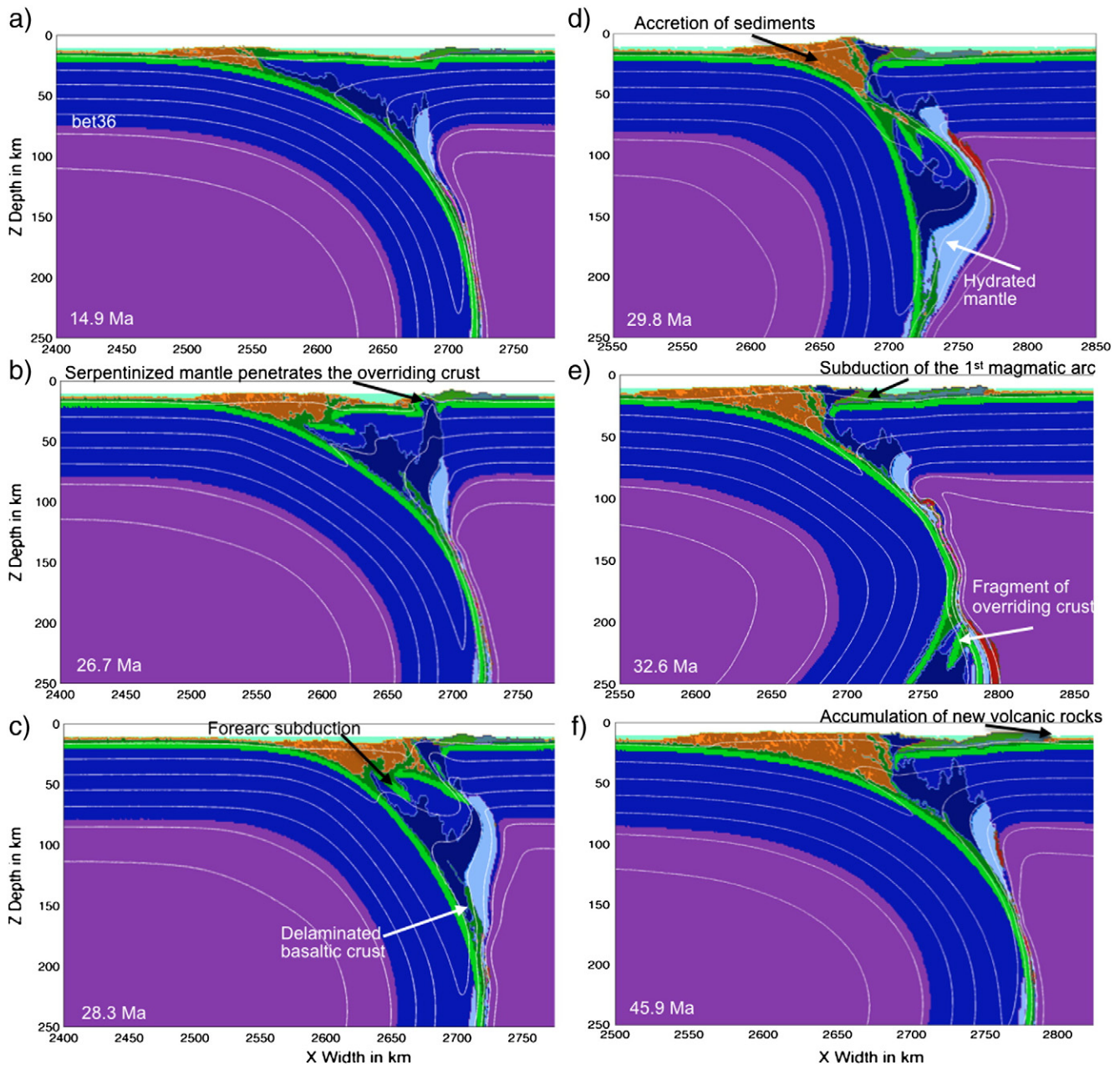


**Fig. 10.** Zoomed area of the reference model bet36 ( $\lambda_{\text{fluid}}=0.1$  and  $\lambda_{\text{melt}}=0.02$ ) with forearc subduction. (a–b) Uprising serpentinized mantle penetrating the overriding lithosphere(c)–(e): Closure of the forearc basin; Two forearc fragments descend to asthenospheric depth; (d) Serpentinized peridotite on the surface. Broad hydrated mantle area with partially molten mantle (red); (e): Subduction of the frontal part of the first arc; (f): Accumulation of new volcanic rocks on the backside of the magmatic arc.

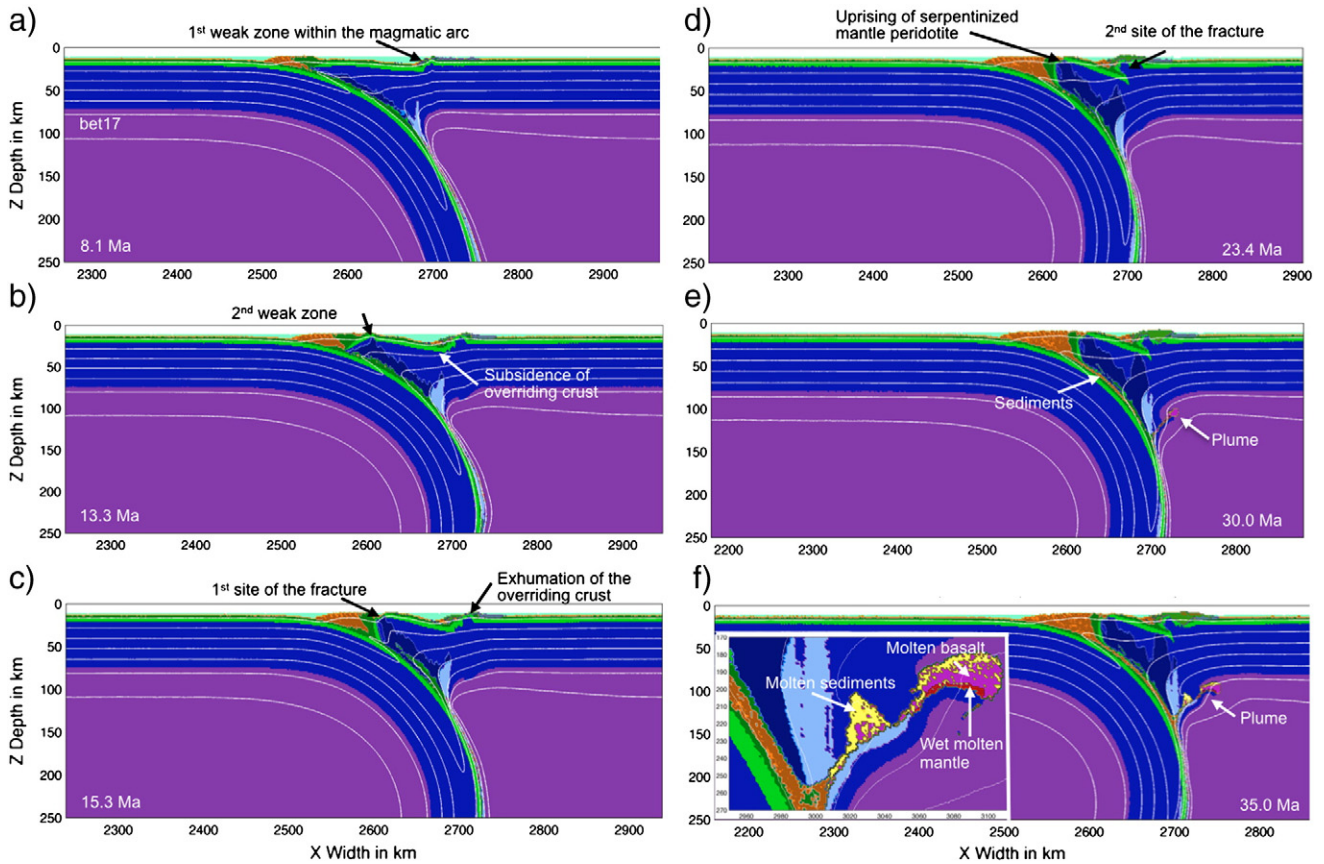


**Fig. 11.** Reference model for a forearc subduction with trans-lithospheric cold plume; ( $\lambda_{\text{fluid}}: 0.3$  and  $\lambda_{\text{melt}}: 0.001$ , model bet17 in Fig. 2). (a): weak zone within the magmatic arc; (b): forearc subsidence; second weak zone; (c): exhumation of overriding crust; first fracture through the overriding plate; (d): second fracture through the overriding plate; (e): subduction of the forearc fragments but stick in the upper part of the mantle; (f): plume rooted in mélange of sediments, basalts and gabbro.

the models with 35 mm/a velocity (Fig. 15). In contrast, the nucleation site of the spreading center seems to be independent of the slab velocity (Fig. 14). In addition, the effect of subducting plate velocity on the accretionary prism geometry, size and dynamics is rather moderate (Fig. 14): more sediment subduction occurred in models with 35 mm/a velocity than in faster experiments, in which sediments are fully scrapped off the subducting plate.

### 3.2.3. Influence of rock cohesion

We emphasized that decreasing the plastic strength of rocks is essentially responsible for coupling/decoupling of the converging oceanic plates. Weakening is here defined with the aforementioned values of  $\lambda_{\text{fluid}}$  and  $\lambda_{\text{melt}}$ . The cohesive strength of rocks (i.e., strength at  $P_{\text{solid}} = 0$ ) was constant (1 MPa) in our experiments. In order to test this parameter, we varied cohesion from 0.1 MPa to 10 MPa in the retreating subduction model bet33 ( $\lambda_{\text{fluid}}: 0.02$  and  $\lambda_{\text{melt}}: 0.02$ ). The explored cohesion variations are within the range of this parameter measured for natural rocks (Brace and Kohlstedt, 1980). Results suggest that the cohesive strength of rocks strongly affects coupling between the plates: decreasing this parameter to 0.1 MPa enhances plate decoupling and speeds up backarc basin development (Figs. 6b and 16a) while increasing cohesion to 10 MPa precludes backarc extension and causes transition from retreating to advancing subduction regimes (Fig. 16a and c).

## 4. Discussion

In our studies three geodynamic regimes of subduction were obtained. They were mainly controlled by plate coupling, which depends on fluid- and melt-related rheological weakening: a) weak

plate coupling and strong fluid related-weakening lead to retreating subduction (Fig. 4), b) intermediate coupling, moderate weakening lead to stable subduction (Fig. 6) and c) strong coupling, lowered weakening result in advancing subduction (Fig. 9). The strong influence of cohesion on the subduction regime (Fig. 16) is related to the fact that this parameter controls strength of fluid and melt-bearing rocks at high degree of weakening (cf. 2.4. Rheological model). Consequently, the increased cohesion, like lowered fluid weakening, causes higher strength of hydrated rocks along the slab interface, thus enhancing plate coupling. Other subduction parameters are less significant: neither the subducting plate velocity nor the age of plates have noticeable influence on the trench movement (Billen and Hirth, 2007).

In agreement with petrological-thermo-mechanical models of oceanic–continental subduction (Gorczyk et al., 2006, 2007a, 2007b; Sizova et al., 2010; Vogt et al., 2012) the aqueous fluids mainly affect the forearc region, while melts weaken the lithosphere below the arc and control extension in the arc region. A backarc basin results either from initially forearc or intra-arc (but not backarc) extension (Fig. 4). This is the direct consequence of fluid and melt weakening that affects two main regions of the overriding plate: the serpentinized forearc weakened by aqueous fluids and the sub-arc lithosphere weakened by melt. Extension obviously nucleates in the weakest region (Fig. 4b). Irrespective of the initial location of extension (i.e., forearc or intra-arc), rapidly produced necking of the overriding plate allows for pronounced decompression melting of the asthenosphere rising into the necking region (Fig. 4d). This triggers slab retreat and formation of a new oceanic lithosphere in the new spreading center. During oceanic floor spreading, a large part of the extended initial arc (intra-arc extension) or the entire

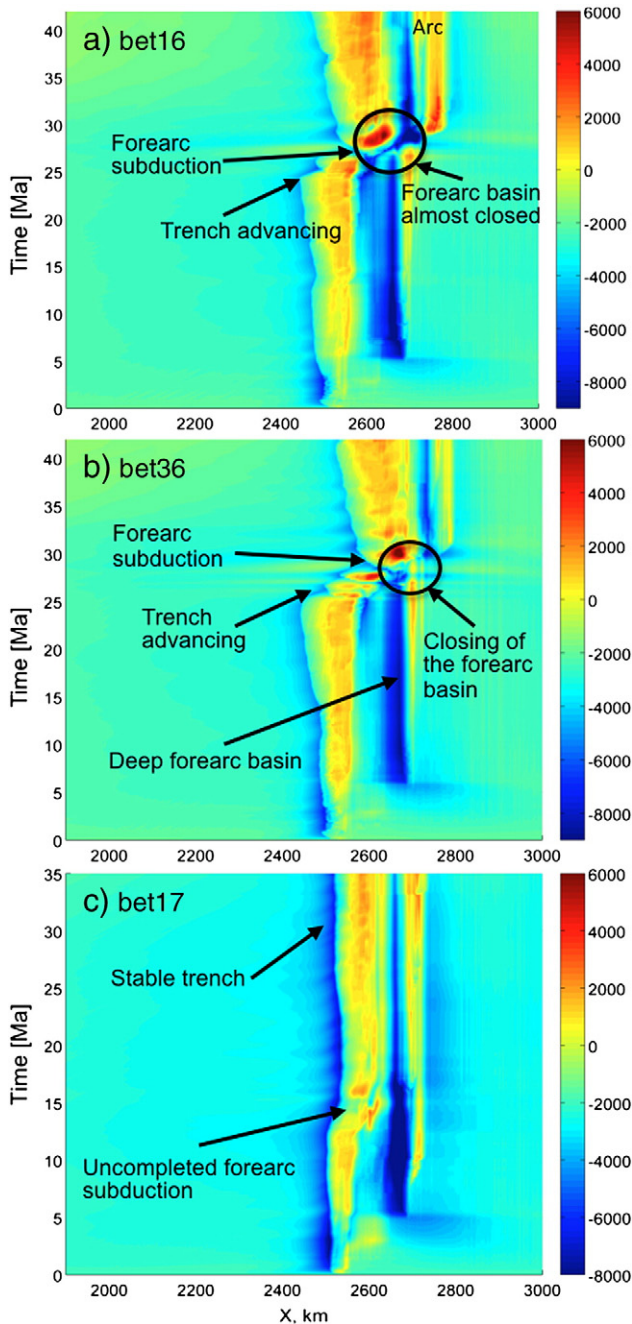


**Fig. 12.** Topography history of the reference models for forearc subduction (Fig. 2). (a) and (b) models bet16 ( $\lambda_{\text{fluid}}=0.1$  and  $\lambda_{\text{melt}}=0.001$  in Fig. 2) and bet36 ( $\lambda_{\text{fluid}}=0.1$  and  $\lambda_{\text{melt}}=0.02$  in Fig. 2) with moderate trench retreat (40–60 km) in ca. 25 Ma and advance of 170–190 km for ca. 5 Ma. Forearc subduction starts about 25 Ma after subduction initiation. (c) Model bet17 ( $\lambda_{\text{fluid}}=0.3$  and  $\lambda_{\text{melt}}=0.001$ ) showing stable trench behavior and incomplete forearc subduction starting 15 Ma after subduction initiation.

initial arc (forearc extension) deactivates and moves away from the trench, thus forming a paleo-arc (Fig. 4e). A younger, active arc forms/remains active on the detached portion of the overriding plate that retreat together with the trench.

On the other hand, differences in the overriding plate composition and structure caused notable differences between our results on intra-oceanic subduction and oceanic–continental subduction models (Gorczyk et al., 2006, 2007a, 2007b; Sizova et al., 2010; Gerya and Meilick, 2011; Vogt et al., 2012). The presence of thin oceanic crust underlain by shallow, partly serpentinized, and fragmented lithospheric mantle in the intra-oceanic forearc region revealed to be

particularly important. A noteworthy result is that, for the first time, we numerically reproduced forearc subduction, which seems to be an unexceptional process for intra-oceanic subduction with strong plate coupling. This process is prompted by intense serpentinization of the shallow forearc mantle, which aids fragmentation and subduction of large lithospheric pieces with the slab. Forearc subduction can be either complete or partial. In the first case, it is often associated with a magmatic pulse caused by dehydration of subducted serpentinized forearc fragments at asthenospheric depths. Note that forearc subduction notably differs from usual subduction erosion (e.g., Von Huene and Scholl, 1991; Vannucchi et al., 2003; Stern, 2011). Subduction erosion is a gradual removal of forearc sediments and crystalline basement by entrainment with the down-going slab (e.g., Von Huene and Scholl, 1991; Stern, 2011). In contrast, forearc subduction (e.g., Boutelier et al., 2011, this study) implies complete, simultaneous subduction of a large fragment of the overriding plate including crust and mantle lithosphere whereas sedimentary wedge may remain almost entirely preserved (Figs. 9, 10).

Our models demonstrate distinct differences in thermal and lithological structure of subduction zones formed in different regimes of intra-oceanic subduction. Particularly strong variations are found in the forearc region where variable degrees of mantle and crustal rock mixing are identified (cf. Figs. 4e, 6d, 7d, 10c and 12c). Variations in the degree of mixing mainly depend on the effective viscosity of the hydrated forearc and can strongly affect the lithological structure of exhumed subduction mélanges (Gerya and Stockhert, 2002). Consequently, exhumed subduction mélanges with intensely intermixed serpentinites, eclogites and sediments may imply reduced viscosity of subduction channel and thus correspond to the conditions of plate decoupling characteristic for either retreating or stable subduction regime (Figs. 4 and 6). This model prediction can thus be used for paleo-tectonic interpretations of subduction-related metamorphic complexes (e.g., Ernst, 1977, 1993; Peacock, 1990; Garrido et al., 2005; Federico et al., 2007; Gorczyk et al., 2007a; Krebs et al., 2008; Blanco-Quintero et al., 2011).

#### 4.1. Comparison with natural subduction systems

Our models of retreating subduction have similarities with regions of active and/or ancient oceanic backarc spreading. These regions generally have an arc close to the trench and a remnant arc on the other side of the back arc basin with a spreading center, for example the Kyushu–Palau Ridge in the Mariana arc system (Stern, 2002; Straub and Zellmer, 2012) and the inactive West Mariana Ridge (Takahashi et al., 2007). Although our experiments are not constrained with the exact parameters of the Izu–Bonin–Mariana subduction system, we find the four characteristic geodynamic features in our general retreating model (Figs. 4, 5b): (i) retreating/advancing trench migration, (ii) an active magmatic arc (e.g. Mariana arc, Izu–Bonin arc), (iii) an active spreading center and backarc basin (e.g. Mariana Trough) and (iv) a paleoarc/remnant arc, which has been separated from the volcanic arc by rifting and spreading (e.g., Kyushu–Palau Ridge, Kodaira et al., 2008), Western Mariana–Ridge Bonin Ridge, (Tatsumi and Stern, 2006; Ishizuka et al., 2010; Tamura et al., 2010). In more details, the internal structure of our evolved retreating subduction model (Fig. 4) is comparable with the geodynamic evolution of the Izu–Bonin arc/backarc system since 50 Ma (Straub, 2003): overriding plate extension associated with moderate subduction angle and convective mantle upwelling is shifted toward the backarc spreading center. In contrast, the 15–7 Ma evolution of the Mariana subduction system (Stern et al., 2003; Straub, 2003) is more similar to our stable subduction models (Figs. 6, 7), in which the trench keeps its position with time, the slab angle is steep and convective mantle upwelling is shifted toward the mantle wedge corner. According to our models, observed contrasts in geodynamic evolution of the neighboring Mariana and Izu–Bonin subduction systems should mainly depend on

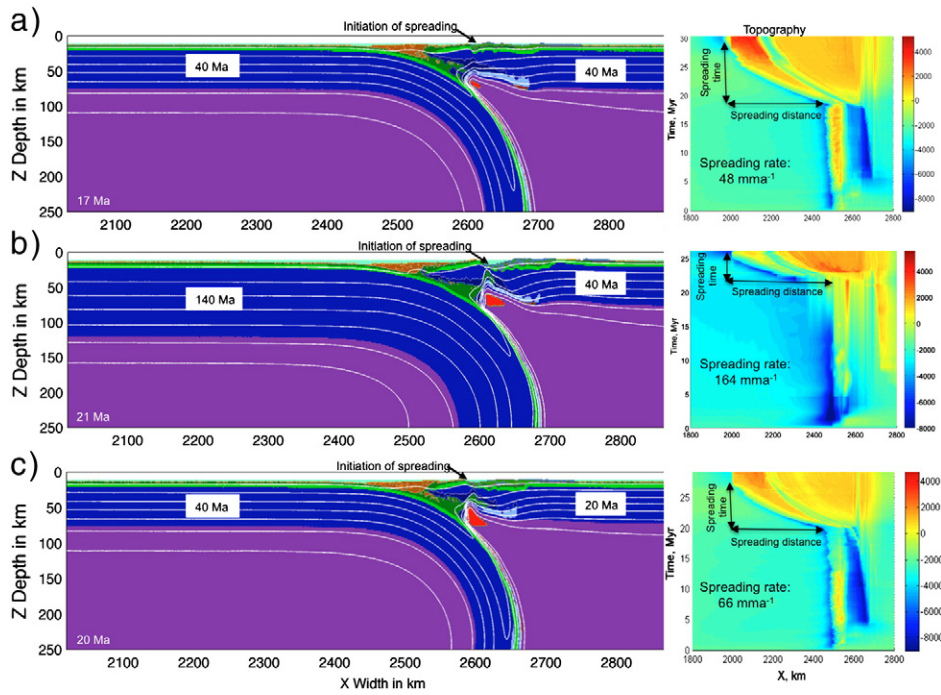


**Fig. 13.** Reference models ( $\lambda_{\text{fluid}}: 0.01$  and  $\lambda_{\text{melt}}: 0.01$ , model bet22 Fig. 2) with different initial ages (framed numbers) of subducting and overriding plates. (a): Similar ages of both plates. Initiation of spreading after 17 Ma. Topography shows spreading rate of  $48 \text{ mm a}^{-1}$ . (b): Contrasting plate ages; Initiation of spreading after 21 Ma. Topography shows spreading rate of  $164 \text{ mm a}^{-1}$ . (c): 20 Ma difference in ages. Initiation of spreading after 20 Ma. Topography shows spreading rate of  $66 \text{ mm a}^{-1}$ .

spatial and temporal variations in the degree of plate coupling. These variations may, in turn, be caused by differences in intensity of fluid- and melt-induced weakening processes, which should correlate with the distribution and intensity of slab dehydration and melt production in the mantle wedge. Documented spatial and temporal variations in the mantle wedge depletion, degree of slab melting and amount of

serpentinite and sediment subduction (e.g. Straub, 2003; Kimura and Yoshida, 2006; Barnes and Straub, 2010) may thus provide keys to observed geodynamic variations.

Other examples for paleoarc/remnant arc are the northern Kohistan Complex (Burg, 2011) and the Nishi-Shichito Ridge in the Izu-Bonin intra-oceanic arc (Kodaira et al., 2008). The geographical sequence of forearc basin, active magmatic arc, backarc spreading occasionally followed by a paleoarc was obtained in the retreating subduction regime (Figs. 7, 8) with a moderate active magmatic arc and no backarc basin and trench migration modeled more the Aleutian type (Ishizuka et al., 2011; Leng and Gurnis, 2011) or an inactive extension regime. The considerable magmatic arcs are typical for the stable subduction models (Fig. 6b,c and d), which could be observed e.g. in the central Aleutians (Jicha et al., 2006).

It is evident that the trench migrates differently in different subduction regimes (Fig. 17). For example the Izu-Bonin-Mariana (IBM) trench migrated recently, after a long time of retreating in an advancing mode (Faccenna et al., 2009) (Fig. 5b). In our experiments, the trench position typically remains relatively stable during the first 20–25 Ma of the model and then may start to migrate either continuously or episodically. With retreating subduction, the average trench retreat velocity varies from 40 to 80 mm/a and is generally slower when retreat is episodically retreating/advancing (Fig. 5 b,c). The extent of trench movements during intermediate advancing stages can reach up to 70 km with the advance rate varying between 40 and 70 mm/a (Fig. 5b). These values match what we know from the Mariana (40–68 mm/a) and Izu-Bonin trenches (65–20 mm/a) (Faccenna et al., 2009). Such episodes in trench behavior are described by Boutelier and Chemenda (2011) in their models and Clark et al. (2008) for the Solomon Sea and Japan. In contrast to observed 10–17 Ma quiescence between advancing/retreating episodes for Lau Basin and Sumatra-Java (Clark et al., 2008), our episodic models did not produce quiescence for longer than 1 to 3 Ma (cf. Fig. 5b and c).

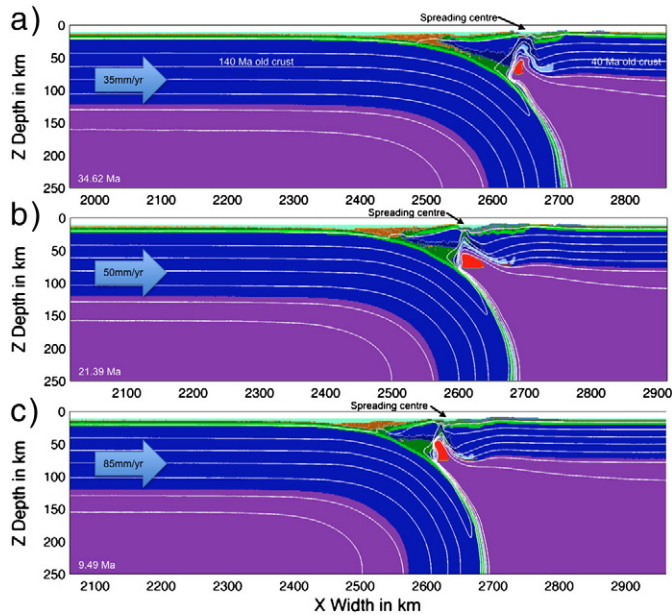


**Fig. 14.** Reference model ( $\lambda_{\text{fluid}}: 0.01$  and  $\lambda_{\text{melt}}: 0.01$ , model bet22 in Fig. 2) with different velocities; (a): Subducting plate velocity of 35 mm/a; Opening of the spreading center at 34.62 Ma; (b): Subducting plate velocity of 50 mm/a; Extension after 21 Ma; (c): Subducting plate velocity of 85 mm/a; Initiation of spreading at 9.49 Ma.

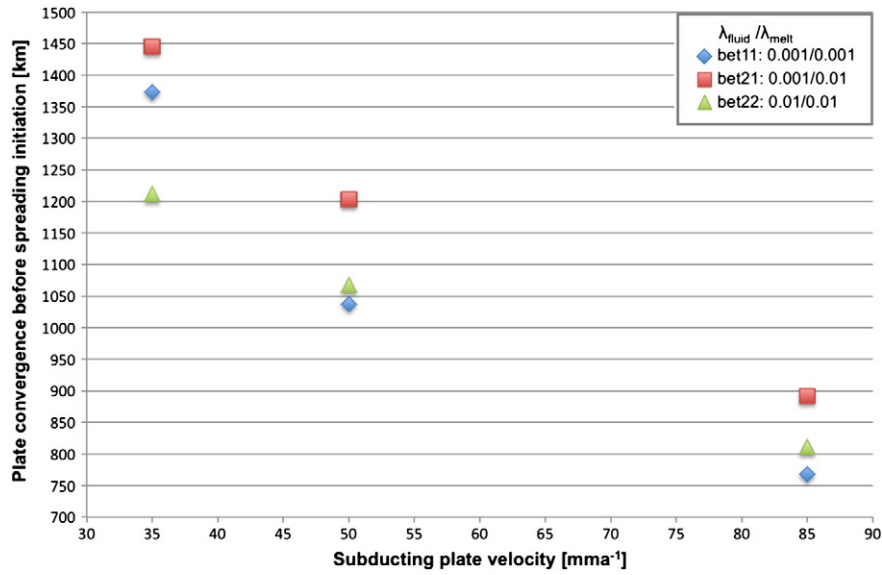


**Fig. 15.** Calculated amount of convergence (y axis) in three experiments (blue:  $\lambda_{\text{fluid}} = 0.001$ ,  $\lambda_{\text{melt}} = 0.001$ , model bet11), red: ( $\lambda_{\text{fluid}} = 0.001$ ,  $\lambda_{\text{melt}} = 0.01$ , model bet21), green: ( $\lambda_{\text{fluid}} = 0.01$ ,  $\lambda_{\text{melt}} = 0.01$ , model bet22) with different subducting plate velocities (x axis: subducting plate velocity (mma<sup>-1</sup>); y axis: plate convergence before spreading initiation). Initiation age in all experiments for subducting plate: 140 Ma and for overriding plate: 40 Ma.

In the case of advancing subduction regime, the rate of trench advance is limited by the prescribed subducting plate velocity and varies between 20 and 40 mm/a. The amplitude of trench advance varies from 20 km when forearc subduction is incomplete to 150 km (Fig. 12c) when forearc subduction is complete (Fig. 12a and b). After 15–30 Ma the trench stops migrating and stays on its new position, as Clark et al. (2008) reported for

Izu–Bonin, Mariana and Japan. Forearc subduction has been inferred in several subduction/collision zones (Oman: Chemenda et al., 2001; Billen, 2010; Ural: Boutelier and Chemenda, 2011) but is not observed in modern intra-oceanic subduction zones. We contend that our models have stronger plate coupling (i.e., insufficient fluid weakening) than current intra-oceanic subduction settings.

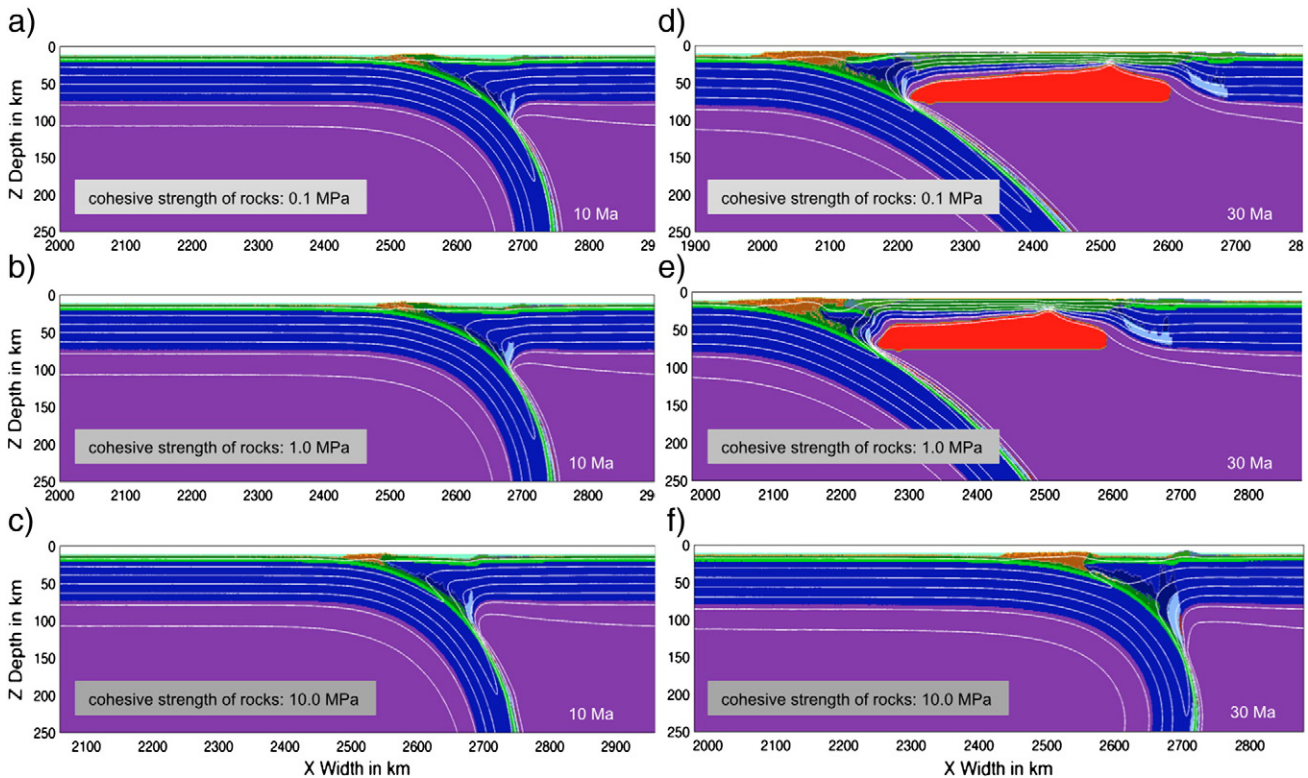


**Fig. 16.** Reference model with different cohesive strength of rocks; ( $\lambda_{\text{fluid}} = 0.02$  and  $\lambda_{\text{melt}} = 0.02$ , model bet33 in Fig. 2). (a)–(c): no difference between the three experiments for the first 10 Ma (d) and (e): After 30 Ma similar development of decompression melting and extension; (f): no extension; well developed arc above a broad area of hydrated (light blue) and serpentinized (dark blue) mantle.

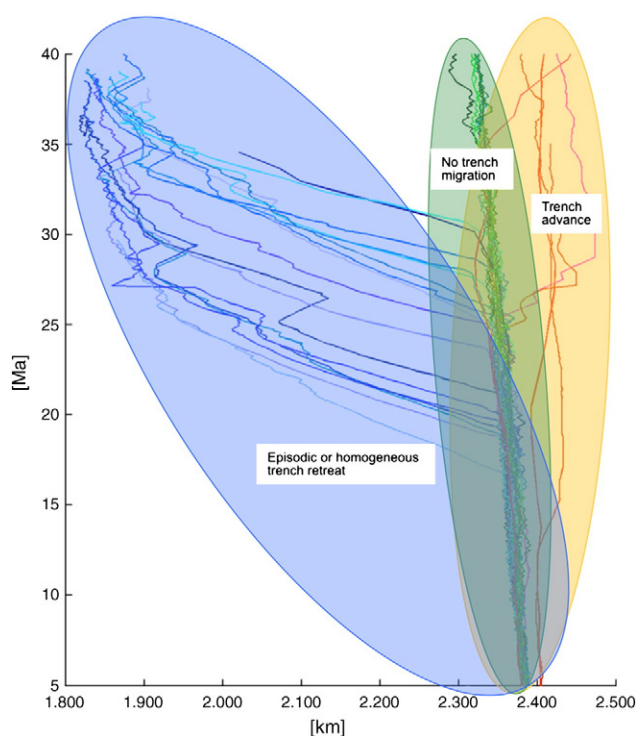


**Fig. 17.** Overview of different trench migrations over ca. 35 Ma. Trenches behave according to the coupling/decoupling. Three directions of trench migration: retreating (blue), stable (green), advancing (yellow). The two axes indicate time (Ma) over distance (km).

Some of our models are characterized by relatively stable trench position and demonstrate neither notable advance nor retreat (Fig. 8). This behavior may, however, be transient since the trench is stable at the beginning of all models and its position may be destabilized by the ongoing subduction processes. Most of these nearly stationary trenches have a very slow retreat behavior due to the gradual accretion of sedimentary wedges in the forearc. Indeed, sediment accretion is generally too intense in our models compared to typical modern intra-oceanic subduction zones (Leat and Larter, 2003). This problem could possibly be improved with the use of more sophisticated erosion/sedimentation models, which is beyond the scope of this study.

## 5. Conclusion

Three main geodynamic regimes of intra-oceanic subduction are identified in numerical thermo-mechanical experiments: retreating subduction with occasional opening of backarc basin, stable subduction, and advancing subduction. The main difference between these regimes is the degree of rheological coupling between plates, which in turn is governed by the intensity of rheological weakening induced by fluids and melts. Neither subducting plate velocity nor ages of the subducting and overriding plates have significant influence on these geodynamic regimes.

Backarc basin formation requires plate decoupling. A spreading center in retreating subduction regime nucleates either in forearc or in the intra-arc region and then separates a deactivated paleo-arc from the active, near-trench arc.

Advancing subduction results from strong plate coupling. At the mature stage, this compressive geodynamic regime leads to complete or partial fragmentation and subduction of the previously serpentinized forearc region.

Episodic trench behavior is characteristic for the retreating subduction regime. It is a consequence of variations of plate coupling with time

caused by (fore) arc deformation processes. This episodicity is not observed for the stable and compressive subduction regimes.

## Acknowledgments

Detailed and constructive reviews of two anonymous reviewers are greatly appreciated. This work was supported by the ETH Research Grants ETH-06 09 -2, Crystal2Plate program, SNF ProDoc program 4-D-Adamello and TopoEurope Program.

## References

- Arcay, D., Tric, E., Doin, M.P., 2005. Numerical simulations of subduction zones – effect of slab dehydration on the mantle wedge dynamics. *Physics of the Earth and Planetary Interiors* 149, 133–153.
- Arcay, D., Lallemand, S., Doin, M.P., 2008. Back-arc strain in subduction zones: statistical observations versus numerical modeling. *Geochemistry, Geophysics, Geosystems* 9. <http://dx.doi.org/10.1029/2007GC001875>.
- Barnes, J.D., Straub, S.M., 2010. Chlorine stable isotope variations in Izu Bonin tephra. Implications for serpentinite subduction. *Chemical Geology* 272, 62–74. <http://dx.doi.org/10.1016/j.chemgeo.2010.1002.1005>.
- Billen, M.I., 2008. Modeling the dynamics of subducting slabs. *Annual Review of Earth and Planetary Sciences* 36, 325–356.
- Billen, M.I., Hirth, G., 2007. Rheologic controls on slab dynamics. *Geochemistry, Geophysics, Geosystems* 8.
- Billen, M.I., 2010. Slab dynamics in the transition zone. *Physics of the Earth and Planetary Interiors* 183, 296–308. <http://dx.doi.org/10.1016/j.pepi.2010.05.005>.
- Bittner, D., Schmeling, H., 1995. Numerical modeling of melting processes and induced diapirism in the lower crust. *Geophysical Journal International* 123, 59–70.
- Blanco-Quintero, I., Garcia-Casco, A., Gerya, T.V., 2011. Tectonic blocks in serpentinite melange (eastern Cuba) reveal large-scale convective flow of the subduction channel. *Geology* 39, 79–82.
- Boutelier, D., Chemenda, A., 2011. Physical modeling of arc–continent collision. A review of 2D, 3D, purely mechanical and thermo-mechanical experimental models, v. arc–continent collision, no. In: Brown, D., Ryan, P.D. (Eds.), *Arc–Continent Collision*. : *Frontiers in Earth Sciences*. Springer-Verlag, Berlin Heidelberg, pp. 445–473.
- Boutelier, D., Chemenda, A., Burg, J.P., 2003. Subduction versus accretion of intra-oceanic volcanic arcs: insight from thermo-mechanical analogue experiments. *Earth and Planetary Science Letters* 212, 31–45.
- Brace, W.F., Kohlstedt, D.L., 1980. Limits on lithospheric stress imposed by laboratory experiments. *Journal of Geophysical Research* 85, 6248–6252.
- Burg, J.P., 2011. The Asia–Kohistan–India collision. Review and discussion, v. Arc–continent collision, no. In: Brown, D., Ryan, P.D. (Eds.), *Arc–Continent Collision*. : *Frontiers in Earth Sciences*. Springer-Verlag, Berlin Heidelberg, pp. 279–309. [http://dx.doi.org/10.1007/978-3-540-88558-0\\_16](http://dx.doi.org/10.1007/978-3-540-88558-0_16).
- Chemenda, A.I., Hurlin, D., Tang, J.C., Stephan, J.F., Buffet, G., 2001. Impact of arc–continent collision on the conditions of burial and exhumation of UHP/LT rocks: experimental and numerical modelling. *Tectonophysics* 342, 137–161.
- Clark, S.R., Stegman, D., Muller, R.D., 2008. Episodicity in back-arc tectonic regimes. *Physics of the Earth and Planetary Interiors* 171, 265–279.
- Clauser, C., Huenges, E., 1995. Thermal conductivity of rocks and minerals. In: Ahrens, T.J. (Ed.), *Rock Physics and Phase Relations*. AGU Reference Shelf 3. American Geophysical Union, Washington DC, pp. 105–126.
- Ernst, W.G., 1977. Mineral parageneses and plate tectonic settings of relatively high-pressure metamorphic belts. *Fortschritte der Mineralogie* 54, 192–222.
- Ernst, W.G., 1993. Metamorphism of Franciscan tectonostratigraphic assemblage, Pacheco Pass area, east-central Diablo Range, California Coast Ranges. *Geological Society of America Bulletin* 105, 618–636.
- Faccenna, C., Di Giuseppe, E., Funicello, F., Lallemand, S., van Hunen, J., 2009. Control of seafloor aging on the migration of the Izu–Bonin–Mariana trench. *Earth and Planetary Science Letters* 288, 386–398.
- Federico, L., Crispini, L., Scambelluri, M., Capponi, G., 2007. Ophiolite melange zone records exhumation in a fossil subduction channel. *Geology* 35, 499–502.
- Garrido, C.J., Sanchez-Vizcaino, V.L., Gomez-Pugnaire, M.T., Trommsdorff, V., Alard, O., Bodinier, J.L., Godard, M., 2005. Enrichment of HFSE in chlorite–harzburgite produced by high-pressure dehydration of antigorite–serpentinite: implications for subduction magmatism. *Geochemistry, Geophysics, Geosystems* 6. <http://dx.doi.org/10.1029/2004GC000791>.
- Gerya, T.V., Meilick, F.I., 2011. Geodynamic regimes of subduction under an active margin: effects of rheological weakening by fluids and melts. *Journal of Metamorphic Geology* 29, 7–31.
- Gerya, T.V., Stockhert, B., 2002. Exhumation rates of high pressure metamorphic rocks in subduction channels: the effect of rheology. *Geophysical Research Letters* 29, 102-1–102-4.
- Gerya, T.V., Yuen, D.A., 2003a. Rayleigh–Taylor instabilities from hydration and melting propel ‘cold plumes’ at subduction zones. *Earth and Planetary Science Letters* 212, 47–62.
- Gerya, T.V., Yuen, D.A., 2003b. Characteristics-based marker-in-cell method with conservative finite-differences schemes for modeling geological flows with strongly variable transport properties. *Physics of the Earth and Planetary Interiors* 140, 293–318.

- Gerya, T.V., Yuen, D.A., 2007. Robust characteristics method for modelling multiphase visco-elasto-plastic thermo-mechanical problems. *Physics of the Earth and Planetary Interiors* 163, 83–105.
- Gerya, T.V., Stockhert, B., Perchuk, A.L., 2002. Exhumation of high-pressure metamorphic rocks in a subduction channel. A numerical simulation. *Tectonics* 21, 6–1–15.
- Gorczyk, W., Gerya, T.V., Connolly, J.A.D., Yuen, D.A., Rudolph, M., 2006. Large-scale rigid-body rotation in the mantle wedge and its implications for seismic tomography. *Geochemistry, Geophysics, Geosystems* 7. <http://dx.doi.org/10.1029/2005GC001075>.
- Gorczyk, W., Guillot, S., Gerya, T.V., Hattori, K., 2007a. Asthenospheric upwelling, oceanic slab retreat, and exhumation of UHP mantle rocks: insights from Greater Antilles. *Geophysical Research Letters* 34. <http://dx.doi.org/10.1029/2007GL031059>.
- Gorczyk, W., Willner, A.P., Gerya, T.V., Connolly, J.A.D., Burg, J.P., 2007b. Physical controls of magmatic productivity at Pacific-type convergent margins numerical modelling. *Physics of the Earth and Planetary Interiors* 163, 209–232.
- Hebert, L.B., Antoshechkina, P., Asimov, P., Gurnis, M., 2009. Emergence of a low-viscosity channel in subduction zones through the coupling of mantle flow and thermodynamics. *Earth and Planetary Science Letters* 278, 243–256.
- Hess, P.C., 1989. *Origin of Igneous Rocks*. Harward University Press, London, UK.
- Hirschmann, M.M., 2000. Mantle solidus: experimental constraints and the effects of peridotite composition. *Geochemistry Geophysics Geosystems* 1 (1–21), 1042.
- Hofmeister, A.M., 1999. Mantle values of thermal conductivity and the geotherm from phonon lifetimes. *Science* 283, 1699–1706.
- Ishizuka, O., Yuasa, M., Tamura, Y., Shukuno, H., Stern, R.J., Naka, J., Joshima, M., Taylor, R.N., 2010. Migrating shoshonitic magmatism tracks Izu–Bonin–Mariana intra-oceanic arc rift propagation. *Earth and Planetary Science Letters* 294, 111–122.
- Ishizuka, O., Taylor, R.N., Yuasa, M., Ohara, Y., 2011. Making and breaking an island arc: a new perspective from the Oligocene Kyushu–Palau arc, Philippine Sea. *Geochemistry, Geophysics, Geosystems* 12.
- Jicha, B.R., Scholl, D.W., Singer, B.S., Yogodzinski, G.M., Kay, S.M., 2006. Revised age of Aleutian Island Arc formation implies high rate of magma production. *Geology* 34, 661–664.
- Johannes, W., 1985. The significance of experimental studies for the formation of migmatites. In: Ashworth, J.R. (Ed.), *Migmatites*. Blackie, Glasgow, UK, pp. 36–85.
- Kimura, J., Yoshida, T., 2006. Contributions of slab fluid, mantle 1576 wedge and crust to the origin of quaternary lavas in the NE 1577 Japan arc. *Journal of Petrology* 47, 2185–2232.
- Kodaira, S., Sato, T., Takahashi, N., Miura, S., Tamura, Y., Tatsumi, Y., Kaneda, Y., 2007. New seismological constraints on growth of continental crust in the Izu–Bonin intra-oceanic arc. *Geology* 35, 1031–1034.
- Kodaira, S., Sato, T., Takahashi, N., Yamashita, M., No, T., Kaneda, Y., 2008. Seismic imaging of a possible paleoarc in the Izu–Bonin intraoceanic arc and its implications for arc evolution processes. *Geochemistry, Geophysics, Geosystems* 9. <http://dx.doi.org/10.1029/2008GC002073>.
- Kodaira, S., Noguchi, N., Takahashi, N., Ishizuka, O., Kaneda, Y., 2010. Evolution from fore-arc oceanic crust to island arc crust: a seismic study along the Izu–Bonin fore arc. *Journal of Geophysical Research* 115. <http://dx.doi.org/10.1029/2009JB006968>.
- Krebs, M., Maresch, W.V., Schertl, H.P., Muenker, C., Baumann, A., Draper, G., Idleman, B., Trapp, E., 2008. The dynamics of intra-oceanic subduction zones: A direct comparison between fossil petrological evidence (Rio San Juan Complex, Dominican Republic) and numerical simulation. *Lithos* 103, 106–137.
- Lallemand, S., Heuret, A., Faccenna, C., Funicello, F., 2008. Subduction dynamics as revealed by trench migration. *Tectonics* 27. <http://dx.doi.org/10.1029/2007TC002212>.
- Leat, P.T., Larter, R.D., 2003. Intra-oceanic subduction systems: introduction. *Geological Society, London, Special Publications* 219, 1–17.
- Leng, W., Gurnis, M., 2011. Dynamics of subduction initiation with different evolutionary pathways. *Geochemistry, Geophysics, Geosystems* 12.
- Miller, M.S., Kennett, B.L.N., Toy, V.G., 2006. Spatial and temporal evolution of the subducting Pacific plate structure along the western Pacific margin. *Journal of Geophysical Research* 111. <http://dx.doi.org/10.1029/2005JB003705>.
- Nikolaeva, K., Gerya, T.V., Connolly, J.A.D., 2008. Numerical modelling of crustal growth in intraoceanic volcanic arcs. *Physics of the Earth and Planetary Interiors* 171, 336–356.
- Peacock, S.M., 1990. Numerical-simulation of metamorphic pressure–temperature–time paths and fluid production in subducting slabs. *Tectonics* 9, 1197–1211.
- Poli, S., Schmidt, M.W., 2002. Petrology of subducted slabs. *Annual Review of Earth and Planetary Sciences* 30, 207–235.
- Ranalli, G., 1995. *Rheology of the Earth*. Chapman and Hall, London, UK.
- Ruepke, L.H., Morgan, J.P., Hort, M., Connolly, J.A.D., 2004. Serpentine and the subduction zone water cycle. *Earth and Planetary Science Letters* 223, 17–34.
- Schmeling, H., Babeyko, A.Y., Enns, A., Faccenna, C., Funicello, F., Gerya, T.V., Golabek, G.J., Griggull, S., Kaus, B.J.P., Morra, G., Schmalholz, S.M., van Hunen, J., 2008. A benchmark comparison of spontaneous subduction models—towards a free surface. *Physics of the Earth and Planetary Interiors* 171, 198–223.
- Schmidt, M.W., Poli, S., 1998. Experimentally based water budgets for dehydrating slabs and consequences for arc magma generation. *Earth and Planetary Science Letters* 163, 361–379.
- Sdrolias, M., Muller, R.D., 2006. Controls on back-arc basin formation. *Geochemistry, Geophysics, Geosystems* 7. <http://dx.doi.org/10.1029/2005GC001090>.
- Sizova, E., Gerya, T.V., Brown, M., Perchuk, L.L., 2010. Subduction styles in the Precambrian: insight from numerical experiments. *Lithos* 116, 209–229.
- Stern, R.J., 2002. Subduction zones. *Reviews of Geophysics* 3–1–38.
- Stern, C.R., 2011. Subduction erosion: rates, mechanisms, and its role in arc magmatism and the evolution of the continental crust and mantle. *Gondwana Research* 20, 284–308.
- Stern, R.J., Fouch, M., Klemperer, S.L., 2003. An overview of the Izu–Bonin–Mariana subduction factory. *Geophysical Monograph* 138.
- Straub, S.M., 2003. The evolution of the Izu Bonin–Mariana volcanic arcs (NW Pacific) in terms of major element chemistry. *Geochemistry, Geophysics, Geosystems* 4.
- Straub, S.M., Zellmer, G.F., 2012. Volcanic arcs as archives of plate tectonic change. *Gondwana Research* 21, 495–516. <http://dx.doi.org/10.1016/j.jgr.2011.10.006>.
- Takahashi, N., Kodaira, S., Klemperer, S.L., Tatsumi, Y., Kaneda, Y., Suyehiro, K., 2007. Crustal structure and evolution of the Mariana intra-oceanic island arc. *Geology* 203–206.
- Takahashi, N., Kodaira, S., Tatsumi, Y., Kaneda, Y., Suyehiro, K., 2008. Structure and growth of the Izu–Bonin–Mariana arc crust: 1. Seismic constraint on crust and mantle structure of the Mariana arc-back-arc system. *Journal of Geophysical Research* 113. <http://dx.doi.org/10.1029/2007JB005120>.
- Takahashi, N., Kodaira, S., Tatsumi, Y., Yamashita, M., Sato, T., Kaiho, Y., Miura, S., No, T., Takizawa, K., Kaneda, Y., 2009. Structural variations of arc crusts and rifted margins in the southern Izu–Ogasawara arc-back arc system. *Geochemistry, Geophysics, Geosystems* 10. <http://dx.doi.org/10.1029/2008GC002146>.
- Tamura, Y., Ishizuka, O., Aoike, K., Kawate, S., Kawabata, H., Chang, Q., Saito, S., Tatsumi, Y., Arima, M., Takahashi, M., Kanamaru, T., Kodaira, S., Fiske, R.S., 2010. Missing oligocene crust of the Izu–Bonin arc: consumed or rejuvenated during collision? *Journal of Petrology* 51, 823–846.
- Tatsumi, Y., Stern, C.R., 2006. Manufacturing continental crust in the subduction factory. *Oceanography* 19, 4.
- Turcotte, D.L., Schubert, G., 2002. *Geodynamics*. Cambridge University Press, Cambridge, UK.
- Vannucchi, P., Ranero, C., Galeotti, S., Straub, S., Scholl, D., McDougall-Ried, K., 2003. Fast rates of subduction erosion along the Costa Rica Pacific margin: Implications for nonsteady rates of crustal recycling at subduction zones. *Journal of Geophysical Research* 108 (B11). <http://dx.doi.org/10.1029/2002JB002207>.
- Vogt, K., Gerya, T.V., Castro, A., 2012. Crustal growth at active continental margins: numerical Modeling. *Physics of the Earth and Planetary Interiors* 192–193, 1–20.
- Von Huene, R., Scholl, D.W., 1991. Observations at convergent margins concerning sediment subduction, subduction erosion, and the growth of continental-crust. *Reviews of Geophysics* 29, 279–316.
- Zhu, G., Gerya, T.V., Yuen, D.A., Honda, S., Yoshida, T., Connolly, J.A.D., 2009. Three-dimensional dynamics of hydrous thermal–chemical plumes in oceanic subduction zones. *Geochemistry, Geophysics, Geosystems* 10. <http://dx.doi.org/10.1029/2009GC002625>.
- Zhu, G., Gerya, T.V., Honda, S., Tackley, P.J., Yuen, D.A., 2011. Influences of the buoyancy of partially molten rock on 3-D plume patterns and melt productivity above retreating slabs. *Physics of the Earth and Planetary Interiors* 185, 112–121.